Journal of Computational Physics 229 (2010) 6623–6643

Contents lists available at ScienceDirect

Journal of Computational Physics

journal homepage: www.elsevier.com/locate/jcp

A Trefftz-based numerical modelling framework for Helmholtz problems with complex multiple-scatterer configurations

Bert Van Genechten *, Bart Bergen, Dirk Vandepitte, Wim Desmet

K.U.Leuven, Department of Mechanical Engineering, Celestijnenlaan 300B, Box 2420, 3001 Heverlee (Leuven), Belgium

ARTICLE INFO

Article history:
Received 30 June 2009
Received in revised form 17 May 2010
Accepted 20 May 2010
Available online 26 May 2010

Keywords:
Multiple-scattering
Helmholtz equation
Unbounded domain
Mid-frequency
Trefftz method
Wave Based Method

ABSTRACT

The aim of the work presented in this paper is the numerical solution of low- and mid-frequency time-harmonic acoustic multiple-scattering problem. A novel so-called 'multi-level' modelling approach is proposed which is applicable to the study of a configuration of well separated obstacles of arbitrary shape on which any type of acoustic boundary condition can be applied. The generic character of the method is obtained by embedding the superposition principle for the multiple-scattering influence in a state-of-the-art acoustic modelling technique, the so-called Wave Based Method. The resulting approach successfully alleviates the geometrical limitations of the underlying Trefftz-based method and preserves the method's computational efficiency, resulting in a generic multiple-scattering modelling framework with a superior computational efficiency in the low- as well as the mid-frequency range. Several numerical validation examples show that the proposed approach is as accurate as the classical single-scattering Wave Based Method and illustrate the computational efficiency as compared to Boundary Element Methods.

1. Introduction

In recent years, the problem of efficiently solving multiple-scattering problems has received considerable attention in a broad range of areas of applied sciences like acoustics, electromagnetism, elasticity and marine engineering. The aim of these research efforts is to devise efficient and robust numerical methods which allow the study of the scattering behaviour of general configurations of arbitrarily shaped obstacles. The scattering field in a multiple-scattering problem results from the complex interaction between the incident excitation fields and the separate obstacles on the one hand and between the different scatterers on the other hand. The strength and nature of these interactions depend largely on the shape and surface properties of the obstacles, their relative position with respect to each other and the physical properties of the surrounding medium. Due to the complex nature of these phenomena, the development of numerical methods to study this type of problems requires special attention, especially when a large number of obstacles is present and/or when the frequency of interest is high.

The main interest of the research presented in this paper is to model the time-harmonic acoustic scattering behaviour of a large scatterer which is composed of many distinct smaller scattering objects. In order to attain this goal a general modelling framework is needed which allows the solution of the Helmholtz equation in an unbounded medium which contains objects with arbitrary shapes and properties. A wide variety of approaches to solve this problem can be found in literature. For an extensive overview of these techniques, the reader is referred to the textbook [1] by Martin. Many of the proposed methods

* Corresponding author. Tel.: +32 16 32 86 06; fax: +32 16 32 29 87.
E-mail address: Bert.VanGenechten@mech.kuleuven.be (B. Van Genechten).

0021-9991/$ - see front matter © 2010 Elsevier Inc. All rights reserved.
doi:10.1016/j.jcp.2010.05.016

are either based on an integral equation formulation of the multiple-scattering problem [2,3] or on an expansion of the scattered field as a superposition of multipoles related to circular (or spherical) scatterer geometries [4–7]. The former approach has the advantage of being (theoretically) applicable to generally shaped problem geometries and allows to incorporate arbitrary boundary conditions in the numerical models. The drawback is however that these methods involve elaborate (and often problem-specific) theoretical derivations such that the development of a generic method of this type is not straightforward. The latter approach is based on the superposition principle for the scattered field and combines analytical *T*-matrix formulations for each individual scatterer with the associated translation formulas to express the mutual coupling between multiple scatterers [8]. Originally, these formulations were derived for simple geometries, such as cylinders, spheres, ellipses and ellipsoids and their computational efficiency tends to break down if the geometry of the scatterer under study deviates significantly from these basic shapes. The applicability of the method can be extended to more general geometries by either using alternative (numerical) approaches such as classical Boundary Element Methods to derive the *T*-matrix for each individual scatterer [9] or by decomposing the scatterer boundary into small segments which can be approximated by these simpler shapes and applying a recursive aggregated *T*-matrix algorithm to derive the *T*-matrix for the complete scatterer [10]. The main challenges for this approach are the search for efficient numerical solution algorithms to solve the resulting systems of equations [11], the enhancement of the class of scatterer geometries which can be efficiently modelled and the incorporation of general boundary conditions into the formulation such as, e.g. random acoustic pressure, velocity or normal impedance distributions.

The main focus of this paper is on the development of a generic numerical methodology to solve two-dimensional time-harmonic acoustic scattering problems in which complex configurations of arbitrarily shaped scatterers are involved. In the approach presented here, the generic character of the method is realised by integrating the multiple-scatterer interactions in an existing numerical modelling framework. The most commonly applied numerical methodologies for the analysis of general two-dimensional steady-state acoustic problems are deterministic element-based modelling techniques which belong to either the family of the domain or the boundary discretisation methods:

- Of the *boundary discretisation methods*, the Boundary Element Method [12] (BEM), which is based on a boundary integral formulation of the problem, is a well-established numerical technique. Within the applied boundary element discretisation, some acoustic boundary variables are expressed in terms of simple, polynomial shape functions. Enforcing the boundary conditions results in a small numerical model. Since the boundary integral formulation and associated Green's functions inherently satisfy the Sommerfeld radiation condition the BEM does not require particular treatments to handle unbounded domains. Moreover, since only the boundary of the scatterers needs to be discretised, this technique is inherently adapted to the study of multiple-scattering problems.
- Within the family of *domain discretisation methods*, both the Finite Element Method [13] (FEM) and the Finite Difference Method [14] (FDM) are well established. Both methods discretise the problem domain into a large but finite number of small elements. Within these elements, the dynamic response variables, being the acoustic pressure or some derived variables, are described in terms of simple, usually polynomial shape functions. A difficulty in the application of domain discretisation based methods for multiple-scattering problems lies in the effective treatment of unbounded domains, since these techniques model the entire problem domain. In order to overcome this limitation an artificial boundary Γ_t is introduced to truncate the unbounded problem into a bounded problem which encloses all the separate obstacles and inhomogeneities. Special techniques are then required to reduce spurious reflection of waves at the truncation boundary, which results in an exact or approximate representation of a purely outward travelling acoustic wave field along Γ_t. The region between the problem boundary and the truncation boundary is modelled using conventional FEM or FDM techniques. Three strategies are commonly applied in reducing the spurious reflections [15]: non-reflecting boundary conditions (NRBCs) like the well-known Dirichlet-to-Neumann mapping (DtN) [16,17], infinite elements (IEs) [18–20] or perfectly matched layers (PMLs) [21,22].
  If the scatterer consists of several obstacles, which can be well separated from each other, the use of a single artificial boundary Γ_t to enclose the entire scattering region, becomes too expensive. Instead it is preferable to enclose every sub-scatterer j by a separate artificial boundary Γ_t^j. A boundary condition on $\Gamma_t' = \cup\Gamma_t^j$ is then needed to restore the mutual interactions between the sub-scatterers in the numerical model. This boundary condition must not only allow outgoing waves to leave the computational domains without spurious reflections at the artificial boundary, but also propagate the outgoing wave from sub-scatterer j to all other sub-domains, which it may reenter subsequently. To derive such an exact boundary condition, an expression for the solution everywhere in the exterior region is needed. Neither non-reflecting boundary conditions, nor perfectly matched layers provide such a representation, making these methods unfeasible for a partitioned solution approach of a multiple-scattering problem. Of the infinite element and DtN approaches, to the authors' knowledge only the latter has been extended to cope with multiple well separated scatterers [23,24]. In this approach, the resulting acoustic field in the exterior region is described by a Fourier series representation based on a set of close-fitting artificial circular truncation boundaries around each of the scatterers.

The methods described above share the property that they all apply approximating (usually polynomial) functions to represent the spatial variations of the acoustic variables. Since these shape functions are no exact solutions of the governing differential equations, a very fine discretisation is required to suppress the associated pollution error [25] needed to obtain a reasonable prediction accuracy. At high frequencies this requires the solution of very large numerical models, which is

prohibitive due to the lack of sufficient computational resources. As a result, these techniques are limited to low-frequency applications [26,27].

Since many of the interesting phenomena in multiple-scatterer problems occur at frequencies beyond the limiting frequencies of the element-based methods described above, an alternative more efficient modelling technique is needed to form the basis of the envisaged modelling framework. The Wave Based Method (WBM) [28] is a deterministic technique for the analysis of steady-state time-harmonic vibro-acoustic problems. The method is based on an indirect Trefftz approach [29], in that the dynamic response variables are described using wave functions which exactly satisfy the governing differential equation. However, the wave functions may violate the boundary and continuity conditions. Enforcing the residual boundary and continuity errors to zero in a weighted residual scheme yields a small matrix equation. Solution of this matrix equation results in the contribution factors of the wave functions used in the expansion of the dynamic field variables. The WBM has been applied successfully for many steady-state structural dynamic problems [30,31], interior acoustic problems [32] and interior vibro-acoustic problems [33]. This technique has also been successfully extended to exterior acoustic problems [34] through the introduction of an artificial truncation boundary and the use of a special set of scattering wave functions to explicitly describe the acoustic pressure field in the exterior domain. It is shown that, due to the small model size and the enhanced convergence characteristics, the WBM has a superior numerical performance as compared to the element-based methods. As a result, problems at higher frequencies may be tackled.

This paper discusses a new modelling concept for acoustic radiation and scattering problems, particularly suited for the treatment of problems involving multiple distinct scatterers. Like in the multiple-scattering DtN- [23] and *T*-matrix [11] approaches, the total acoustic scattering problem is decomposed into a set of coupled single-scattering problems, each of which is linked to a single object in the configuration. These individual problems are treated separately by the classical WBM methodology for unbounded problems. Application of the addition theorem in the domain between the different truncation boundaries for each of the scatterers and modification of the weighted residual formulation underlying the WBM method results in a system of algebraic equations which governs the original multiple-scattering problem. The outline of this paper is the following: Sections 2 and 3 briefly address the general acoustic problem setting and describe the WB modelling methodology for two-dimensional unbounded acoustic problems. Section 4 is devoted to the discussion of the new multi-level modelling concept, which incorporates multiple scattering in the WB methodology. In Section 5 the new method is applied to a number of examples, in order to both illustrate its potential and validate the accuracy of the obtained results. Finally, Section 6 concludes the paper with general remarks and some possible topics for future research.

2. Problem definition

Consider a general 2D unbounded acoustic problem shown in Fig. 1. The steady-state acoustic pressure inside the problem domain Ω is governed by the inhomogeneous Helmholtz equation:

$$\nabla^2 p(\mathbf{r}) + k^2 p(\mathbf{r}) = -j\rho_0 \omega \delta(\mathbf{r}, \mathbf{r_q}) q, \quad \mathbf{r} \in \Omega \tag{1}$$

with ω the circular frequency and $k = \omega/c$ the acoustic wave number. The acoustic fluid is characterised by the density ρ_0 and the speed of sound c. The fluid is excited by a cylindrical acoustic volume velocity source q. Throughout this article, a harmonic time dependence $e^{j\omega t}$ of the dynamic quantities and excitations is assumed. The problem boundary Γ consists of two parts: the finite part of the boundary, Γ_b, which constitutes the boundary of all the obstacles, and the boundary at infinity, Γ_∞. Based on the three types of commonly applied acoustic boundary conditions, the finite boundary can be further divided into three non-overlapping parts: $\Gamma_b = \Gamma_v \cup \Gamma_p \cup \Gamma_Z$, on which Neumann, Dirichlet and Robin type boundary conditions are applied respectively. If we define the velocity operator $\mathcal{L}_v(\bullet)$, which relates the acoustic normal velocity to the acoustic pressure field, as:

$$\mathcal{L}_v(\bullet) = \frac{j}{\rho_0 \omega} \frac{\partial \bullet}{\partial n}, \tag{2}$$

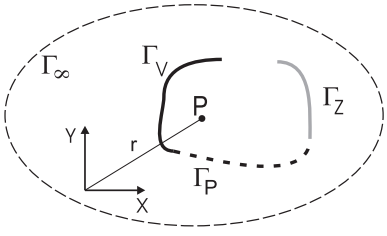

Fig. 1. A general 2D unbounded acoustic problem.

we can write these boundary conditions as:

$$\text{Neumann conditions}: \quad \mathcal{L}_v(p(\boldsymbol{r})) = \bar{v}_n(\boldsymbol{r}), \quad \boldsymbol{r} \in \Gamma_v, \tag{3}$$

$$\text{Dirichlet conditions}: \quad p(\boldsymbol{r}) = \bar{p}(\boldsymbol{r}), \quad \boldsymbol{r} \in \Gamma_p, \tag{4}$$

$$\text{Robin conditions}: \quad \frac{p(\boldsymbol{r})}{\mathcal{L}_v(p(\boldsymbol{r}))} = \overline{Z}_n(\boldsymbol{r}), \quad \boldsymbol{r} \in \Gamma_Z, \tag{5}$$

where the quantities $\bar{v}_n$, $\bar{p}$ and $\overline{Z}_n$ are, respectively, the imposed normal velocity, pressure and normal impedance. At the boundary at infinity Γ_∞ the Sommerfeld radiation condition [35] is applied in order to ensure that the acoustic wave field is purely outgoing at infinity:

$$\lim_{|\boldsymbol{r}|\to\infty} \left(\sqrt{\boldsymbol{r}} \left(\frac{\partial p(\boldsymbol{r})}{\partial |\boldsymbol{r}|} + jkp(\boldsymbol{r}) \right) \right) = 0. \tag{6}$$

The Helmholtz equation (1) together with the associated boundary conditions (3)–(6) define a unique dynamic acoustic pressure field $p(\boldsymbol{r})$.

3. Basic concepts of the Wave Based Method

The Wave Based Method (WBM) [28] is a numerical modelling method based on an indirect Trefftz approach [29] for the solution of steady-state acoustic problems in both bounded and unbounded problem domains. Instead of discretising the entire problem domain (or its boundary) in a large number of small elements and using simple approximating polynomials to describe the acoustic pressure variations like in the FEM, FDM or BEM, the WBM modelling concept is based on a partitioning of the problem into a limited number of large subdomains within which the field variables are expressed as an expansion in terms of wave functions, which inherently satisfy the governing equation, the Helmholtz equation (1). The degrees of freedom are the weighting factors of the wave functions in this expansion. Enforcing the boundary conditions along the problem boundaries and continuity conditions on the interfaces between the subdomains using a weighted residual formulation yields a system of linear equations whose solution vector contains the unknown wave function weighting factors.

The general modelling procedure consists of the following steps:

A. Partitioning into subdomains.
B. Selection of the wave functions in the pressure expansion.
C. Construction of the system of equations via a weighted residual formulation of the boundary conditions and the continuity conditions.
D. Solution of the system of equations and postprocessing of the dynamic variables.

3.1. Domain partitioning

Desmet [28] proposes the basic WBM modelling approach. In this work, a set of approximation functions to describe the steady-state acoustic pressure inside a bounded acoustic domain is derived and it is proven that a sufficient condition for the theoretical convergence of the WBM is the convexity of the bounded domain [28]. In a general acoustic problem however, the problem domain may be non-convex requiring the entire problem domain to be partitioned into a number of convex subdomains. If the WBM is applied for unbounded problems, the introduction of an artificial truncation boundary Γ_t restricts the computational domain to a finite region Ω^- [34], much like in the approaches which enable the domain discretisation based modelling strategies to cope with unbounded problems. After this partitioning, the region Ω^- between the truncation boundary and the problem boundary is partitioned into N_Ω non-overlapping, convex subdomains $\Omega^{(\alpha)}$, as is illustrated in Fig. 2. The unbounded region Ω^+ exterior to Γ_t is modelled explicitly as an additional acoustic subdomain $\Omega^{(N_\Omega+1)}$. As a result, the combined interior/exterior acoustic problem domain is partitioned into $N_\Omega + 1$ subdomains: $\Omega = \Omega^- \cup \Omega^+ = \bigcup_{\alpha=1}^{N_\Omega+1} \Omega^{(\alpha)}$.

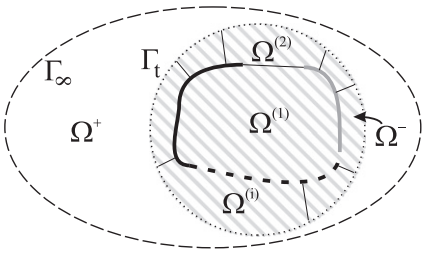

Fig. 2. A WB partitioning of the 2D unbounded problem.

The boundary of each of the acoustic subdomain $\Omega^{(\alpha)}$ is denoted as $\partial\Omega^{(\alpha)}$. It consists of four mutually exclusive parts,

$$\partial\Omega^{(\alpha)} = \Gamma_v^{(\alpha)} \cup \Gamma_Z^{(\alpha)} \cup \Gamma_p^{(\alpha)} \cup \Gamma_I^{(\alpha)}, \tag{7}$$

on which the following conditions apply:

- $\Gamma_v^{(\alpha)} = \Gamma_v \cap \partial\Omega^{(\alpha)}$ indicates the part of the boundary of subdomain $\Omega^{(\alpha)}$ on which normal velocity boundary conditions (3) are applied.
- $\Gamma_p^{(\alpha)} = \Gamma_p \cap \partial\Omega^{(\alpha)}$ indicates the part of the boundary of subdomain $\Omega^{(\alpha)}$ on which pressure boundary conditions (4) are applied.
- $\Gamma_Z^{(\alpha)} = \Gamma_Z \cap \partial\Omega^{(\alpha)}$ indicates the part of the boundary of subdomain $\Omega^{(\alpha)}$ on which normal impedance boundary conditions (5) are applied.
- $\Gamma_I^{(\alpha,\beta)} = \Gamma_I^{(\beta,\alpha)} = \partial\Omega^{(\alpha)} \cap \partial\Omega^{(\beta)}$ indicates the common interface between subdomain $\Omega^{(\alpha)}$ and subdomain $\Omega^{(\beta)}$. The collection of all subdomain interfaces in which subdomain $\Omega^{(\alpha)}$ is involved is denoted as $\Gamma_I^{(\alpha)} = \bigcup_{\beta=1,\beta\neq\alpha}^{N_\Omega+1} \Gamma_I^{(\alpha,\beta)}$.

The boundary of the unbounded acoustic subdomain $\Omega^{(N_\Omega+1)}$ additionally encompasses the boundary at infinity Γ_∞, along which the Sommerfeld radiation condition (6) needs to be fulfilled.

In order to enforce the total resulting acoustic pressure field to be continuous, continuity conditions must be applied at all the interfaces $\Gamma_I^{(\alpha,\beta)}$ between the acoustic subdomains $\Omega^{(\alpha)}$ and $\Omega^{(\beta)}$. To couple the pressure fields in the two subdomains, Pluymers [36] proposes two types of coupling conditions:

- *Pressure–velocity* continuity conditions: In order to obtain a uniquely defined acoustic field which is continuous across the interface between the two subdomains, one continuity condition must be applied on each of the subdomains. Imposing a pressure continuity condition on subdomain $\Omega^{(\alpha)}$ and a normal velocity condition on $\Omega^{(\beta)}$ along the interfaces $\Gamma_{I,p}^{(\alpha,\beta)}$ and $\Gamma_{I,v}^{(\beta,\alpha)}$ is a conventional way to attain this goal:

$$\text{Pressure continuity conditions}: \quad p^{(\alpha)}(\boldsymbol{r}) = p^{(\beta)}(\boldsymbol{r}), \quad \boldsymbol{r} \in \Gamma_{I,p}^{(\alpha,\beta)}, \tag{8}$$

$$\text{Normal velocity conditions}: \quad \mathcal{L}_v^{(\alpha)}(p(\boldsymbol{r})) = -\mathcal{L}_v^{(\beta)}(p(\boldsymbol{r})), \quad \boldsymbol{r} \in \Gamma_{I,v}^{(\beta,\alpha)} \tag{9}$$

  with $\mathcal{L}_v^{(\alpha)}(\bullet) = \frac{j}{\rho_0\omega}\frac{\partial\bullet}{\partial n^{(\alpha)}}$ the velocity operator (2) applied to a point on the boundary of subdomain $\Omega^{(\alpha)}$ and $n^{(\alpha)}$ the normal direction pointing out of $\Omega^{(\alpha)}$.
- *Equivalent normal velocity* continuity conditions: Pluymers [36] proposes an alternative way to couple both acoustic fields. In order to describe these conditions, the following equivalent normal velocity operators are introduced

$$\mathcal{L}_{eq+}^{(\alpha)}(\bullet) = \frac{j}{\rho_0\omega}\frac{\partial\bullet}{\partial n^{(\alpha)}} - \frac{1}{\overline{Z}_{int}}\bullet, \tag{10}$$

$$\mathcal{L}_{eq-}^{(\alpha)}(\bullet) = -\frac{j}{\rho_0\omega}\frac{\partial\bullet}{\partial n^{(\alpha)}} - \frac{1}{\overline{Z}_{int}}\bullet \tag{11}$$

  with $\overline{Z}_{int}$ being an impedance coupling factor.
  The equivalent normal velocity continuity conditions along the boundaries $\Gamma_{I,Z}^{(\alpha,\beta)}$ and $\Gamma_{I,Z}^{(\beta,\alpha)}$ are defined as

$$\mathcal{L}_{eq+}^{(\alpha)}(p^{(\alpha)}(\boldsymbol{r})) = \mathcal{L}_{eq-}^{(\beta)}(p^{(\beta)}(\boldsymbol{r})), \quad \boldsymbol{r} \in \Gamma_{I,Z}^{(\alpha,\beta)}, \tag{12}$$

$$\mathcal{L}_{eq+}^{(\beta)}(p^{(\beta)}(\boldsymbol{r})) = \mathcal{L}_{eq-}^{(\alpha)}(p^{(\alpha)}(\boldsymbol{r})), \quad \boldsymbol{r} \in \Gamma_{I,Z}^{(\beta,\alpha)}. \tag{13}$$

  These continuity conditions result in a more stable formulation than using the conventional conditions enforcing pressure and normal velocity continuity, due to the introduction of damping via $\overline{Z}_{int}$ [37]. Pluymers [36] shows that choosing $\overline{Z}_{int}$ to be the characteristic fluid impedance $\rho_0 c$ is beneficial for the convergence rate of the method.

Since the governing Helmholtz equation is a second order partial differential equation, a single condition needs to be imposed along each of the boundaries of subdomain $\Omega^{(\alpha)}$. As a result, one of the aforementioned types of continuity conditions needs to be selected for each interface linking $\Omega^{(\alpha)}$ to its neighboring subdomains. The choice of the type of condition imposed on each individual interface is however independent such that the basic WBM modelling approach does not prohibit the concurrent use of both types of continuity conditions within a single WBM model as long as the associated parts of the domain boundary $\Gamma_{I,\{p,v\}}^{(\alpha,\beta)}$ and $\Gamma_{I,Z}^{(\alpha,\beta)}$ are non-overlapping. The WBM adopts a direct coupling approach to enforce the coupling conditions described above. This implies that the continuity conditions (8), (9), (12) and (13) are applied directly on the acoustic quantities of the considered subdomains, without introduction of auxiliary variables. In order for the problem to be well-posed, one continuity condition is imposed on each subdomain.

3.2. Field variable expansion

The steady-state acoustic pressure field $p^{(\alpha)}(\boldsymbol{r})$ in each of the acoustic subdomains $\Omega^{(\alpha)}$, $\alpha = 1,\ldots,N_\Omega + 1$ is approximated by a solution expansion $\hat{p}^{(\alpha)}(\boldsymbol{r})$ in terms of $n_w^{(\alpha)}$ acoustic wave functions $\Phi_w^{(\alpha)}$:

$$p^{(\alpha)}(\boldsymbol{r}) \simeq \hat{p}^{(\alpha)}(\boldsymbol{r}) = \sum_{w=1}^{n_w^{(\alpha)}} p_w^{(\alpha)} \Phi_w^{(\alpha)}(\boldsymbol{r}) + \hat{p}_q^{(\alpha)}(\boldsymbol{r}) = \boldsymbol{\Phi}^{(\boldsymbol{\alpha})}(\boldsymbol{r})\boldsymbol{p}_{\boldsymbol{w}}^{(\boldsymbol{\alpha})} + \hat{p}_q^{(\alpha)}(\boldsymbol{r}). \tag{14}$$

The wave function contributions $p_w^{(\alpha)}$ are the weighting factors for each of the selected wave functions $\Phi_w^{(\alpha)}$. Together they form the vector of degrees of freedom $\boldsymbol{p}_{\boldsymbol{w}}^{(\boldsymbol{\alpha})}$. The corresponding a priori defined wave functions are collected in the row vector $\boldsymbol{\Phi}^{(\boldsymbol{\alpha})}$. The set of all $n_W = \sum_{\alpha=1}^{N_\Omega+1} n_w^{(\alpha)}$ acoustic wave function contributions p_w is collected in the column vector $\boldsymbol{p}_{\boldsymbol{w}}$, while the row vector $\boldsymbol{\Phi}$ contains all n_W wave functions. $\hat{p}_q^{(\alpha)}$ represents a particular solution resulting from acoustic source terms $q^{(\alpha)}$ in the right hand side of the inhomogeneous Helmholtz equation (1).

3.2.1. Wave functions for a bounded subdomain

Each acoustic wave function $\Phi_w^{(\alpha)}(\boldsymbol{r})$ exactly satisfies the homogeneous Helmholtz equation (1). For 2D bounded subdomains two types of wave functions which govern the homogeneous part of the Helmholtz equation are distinguished, the *r*- and the *s*-set:

$$\sum_{w=1}^{n_w^{(\alpha)}} p_w^{(\alpha)} \Phi_w^{(\alpha)}(\boldsymbol{r}) = \sum_{w_r=1}^{n_{w_r}^{(\alpha)}} p_{w_r}^{(\alpha)} \Phi_{w_r}^{(\alpha)}(\boldsymbol{r}) + \sum_{w_s=1}^{n_{w_s}^{(\alpha)}} p_{w_s}^{(\alpha)} \Phi_{w_s}^{(\alpha)}(\boldsymbol{r}) \tag{15}$$

with $n_w^{(\alpha)} = n_{w_r}^{(\alpha)} + n_{w_s}^{(\alpha)}$. These wave functions are defined as:

$$\Phi_w^{(\alpha)}(\boldsymbol{r}(x,y)) = \begin{cases} \Phi_{w_r}^{(\alpha)}(x,y) = \cos(k_{xw_r}^{(\alpha)} x) e^{-jk_{yw_r}^{(\alpha)} y}, \\ \Phi_{w_s}^{(\alpha)}(x,y) = e^{-jk_{xw_s}^{(\alpha)} x} \cos(k_{yw_s}^{(\alpha)} y). \end{cases} \tag{16}$$

In order for the wave functions (16) to be exact solutions of (1), they should satisfy the associated dispersion relations:

$$(k_{xw_r}^{(\alpha)})^2 + (k_{yw_r}^{(\alpha)})^2 = (k_{xw_s}^{(\alpha)})^2 + (k_{yw_s}^{(\alpha)})^2 = k^2. \tag{17}$$

As a result, an infinite number of wave functions (16) can be defined for expansion (14). Desmet [28] proposes to select the following wave number components

$$(k_{xw_r}^{(\alpha)}, k_{yw_r}^{(\alpha)}) = \left(\frac{w_1^{(\alpha)}\pi}{L_x^{(\alpha)}}, \pm\sqrt{k^2 - (k_{xw_r}^{(\alpha)})^2} \right), \tag{18}$$

$$(k_{xw_s}^{(\alpha)}, k_{yw_s}^{(\alpha)}) = \left(\pm\sqrt{k^2 - (k_{yw_s}^{(\alpha)})^2}, \frac{w_2^{(\alpha)}\pi}{L_y^{(\alpha)}} \right) \tag{19}$$

with $w_1^{(\alpha)}$ and $w_2^{(\alpha)} = 0, 1, 2, \ldots$ The dimensions $L_x^{(\alpha)}$ and $L_y^{(\alpha)}$ represent the dimensions of the (preferably smallest) bounding rectangle, circumscribing the considered subdomain α.

When a cylindrical volume–velocity source is present in the bounded domain, the free-field acoustic pressure field due to this source at source position $(x_q^{(\alpha)}, y_q^{(\alpha)})$ is added to the solution expansion:

$$\hat{p}_q^{(\alpha)}(x,y) = \frac{\rho_0 \omega q^{(\alpha)}}{4} H_0^{(2)}(k r_q^{(\alpha)}) \tag{20}$$

with $r_q^{(\alpha)} = \sqrt{(x - x_q^{(\alpha)})^2 + (y - y_q^{(\alpha)})^2}$ the distance to the source point and $H_0^{(2)}(\bullet)$ the zero-order Hankel function of the second kind.

3.2.2. Wave functions for an unbounded subdomain

The wave functions for the unbounded domain $\Omega^{(N_\Omega+1)}$ are chosen to implicitly comply with not only the Helmholtz equation (1), but also the Sommerfeld radiation condition (6). This removes the need to explicitly impose a radiation condition, similar to the Green's functions applied in the BEM. Herrera [38] shows that the following expansion yields a complete set of basis functions for a homogeneous Neumann problem exterior to an infinitely long circular cylinder with radius *R*:

$$\sum_{w=1}^{n_w^{(N_\Omega+1)}} p_w^{(N_\Omega+1)} \Phi_w^{(N_\Omega+1)}(\boldsymbol{r}) = p_0^{(N_\Omega+1)} H_0^{(2)}(kr) + \sum_{w=1}^{N} (p_{w_c}^{(N_\Omega+1)} H_w^{(2)}(kr)\cos(w\theta) + p_{w_s}^{(N_\Omega+1)} H_w^{(2)}(kr)\sin(w\theta)) \tag{21}$$

with r and θ polar coordinates, N the number of circumferential orders in the solution expansion ($n_w^{(N_\Omega+1)} = 2N + 1$) and $H_w^{(2)}(\bullet)$ the wth order Hankel function of the second kind. The contributions p_0, p_{w_c} and p_{w_s} are determined by the imposed

velocity distribution along the circumference of the cylinder. From this expansion, the following set of wave functions for unbounded domains is derived:

$$\Phi_w^{(N_\Omega+1)}(\boldsymbol{r}(r,\theta)) = \begin{cases} \Phi_{w_c}^{(N_\Omega+1)}(r,\theta) = H_w^{(2)}(kr)\cos(w\theta), & w = 0,1,2,\ldots, \\ \Phi_{w_s}^{(N_\Omega+1)}(r,\theta) = H_w^{(2)}(kr)\sin(w\theta), & w = 1,2,3,\ldots \end{cases} \tag{22}$$

For modelling sources in unbounded acoustic domains, two source definitions are available [39]. On the one hand, the particular solution for a cylindrical source (20) can be applied. On the other hand, excitation under the form of an acoustic plane wave, travelling at a propagation angle ϕ, is often used for acoustic scattering calculations. The plane wave satisfies the Helmholtz equation (1), and ensures that no reflection occurs at infinity. As a result, the plane wave acoustic pressure field $\hat{p}_{pw}^{(\alpha)}(x,y)$ can be added to the pressure expansion (14) in the same way as a point source:

$$\hat{p}_{pw}^{(\alpha)}(x,y) = e^{jkd(\phi)}, \tag{23}$$

where $d(\phi)$ is the propagation vector of the plane wave.

3.3. Evaluation of boundary and interface conditions

With the use of the basis functions (15) and (21) in the proposed pressure expansion (14), the Helmholtz equation (1) and the Sommerfeld radiation condition (6) are always exactly satisfied, irrespective of the values of the unknown wave function contributions. These contributions only depend on the imposed acoustic boundary and continuity conditions.

Both the boundary and the continuity conditions are defined at an infinite number of boundary positions. Since only finite sized prediction models are amenable to numerical implementation, the boundary and the continuity conditions are, for each subdomain, transformed into a weighted residual formulation. In this formulation, the following definitions for the residual errors are used:

Boundary residuals:

$$\begin{aligned} &\boldsymbol{r} \in \Gamma_v^{(\alpha)} : R_v^{(\alpha)}(\boldsymbol{r}) = \mathcal{L}_v^{(\alpha)}(\hat{p}^{(\alpha)}(\boldsymbol{r})) - \bar{v}_n(\boldsymbol{r}), \\ &\boldsymbol{r} \in \Gamma_Z^{(\alpha)} : R_Z^{(\alpha)}(\boldsymbol{r}) = \mathcal{L}_v^{(\alpha)}(\hat{p}^{(\alpha)}(\boldsymbol{r})) - \frac{\hat{p}^{(\alpha)}(\boldsymbol{r})}{\bar{Z}_n(\boldsymbol{r})}, \\ &\boldsymbol{r} \in \Gamma_p^{(\alpha)} : R_p^{(\alpha)}(\boldsymbol{r}) = \hat{p}^{(\alpha)}(\boldsymbol{r}) - \bar{p}(\boldsymbol{r}). \end{aligned} \tag{24}$$

Interface residuals – *Pressure–velocity coupling*:

$$\begin{aligned} &\boldsymbol{r} \in \Gamma_{l,p}^{(\alpha,\beta)} : R_{l,p}^{(\alpha,\beta)}(\boldsymbol{r}) = \hat{p}^{(\alpha)}(\boldsymbol{r}) - \hat{p}^{(\beta)}(\boldsymbol{r}), \\ &\boldsymbol{r} \in \Gamma_{l,v}^{(\alpha,\beta)} : R_{l,v}^{(\alpha,\beta)}(\boldsymbol{r}) = \mathcal{L}_v^{(\alpha)}(\hat{p}^{(\alpha)}(\boldsymbol{r})) - \mathcal{L}_v^{(\beta)}(\hat{p}^{(\beta)}(\boldsymbol{r})). \end{aligned} \tag{25}$$

Interface residuals – *Equivalent normal velocity coupling*:

$$\boldsymbol{r} \in \Gamma_{l,Z}^{(\alpha,\beta)} : R_{l,Z}^{(\alpha,\beta)}(\boldsymbol{r}) = \mathcal{L}_{eq+}^{(\alpha)}(\hat{p}^{(\alpha)}(\boldsymbol{r})) - \mathcal{L}_{eq-}^{(\beta)}(\hat{p}^{(\beta)}(\boldsymbol{r})). \tag{26}$$

For each subdomain, the error functions are orthogonalised with respect to a weighting function $\tilde{p}^{(\alpha)}$ or its derivative. The weighted residual formulation, applying the introduced error functions for subdomain $\Omega^{(\alpha)}$, is expressed as

$$\begin{aligned} &\int_{\Gamma_v^{(\alpha)}} \tilde{p}^{(\alpha)}(\boldsymbol{r}) R_v^{(\alpha)}(\boldsymbol{r}) \mathrm{d}\Gamma + \int_{\Gamma_Z^{(\alpha)}} \tilde{p}^{(\alpha)}(\boldsymbol{r}) R_Z^{(\alpha)}(\boldsymbol{r}) \mathrm{d}\Gamma + \int_{\Gamma_p^{(\alpha)}} -\mathcal{L}_v^{(\alpha)}(\tilde{p}^{(\alpha)}(\boldsymbol{r})) R_p^{(\alpha)}(\boldsymbol{r}) d\Gamma \\ &+ \sum_{\beta=1,\beta\neq\alpha}^{N_\Omega+1} \left[\int_{\Gamma_{l,p}^{(\alpha,\beta)}} -\mathcal{L}_v^{(\alpha)}(\tilde{p}^{(\alpha)}(\boldsymbol{r})) R_{l,p}^{(\alpha,\beta)}(\boldsymbol{r}) \mathrm{d}\Gamma + \int_{\Gamma_{l,v}^{(\alpha,\beta)}} \tilde{p}^{(\alpha)}(\boldsymbol{r}) R_{l,v}^{(\alpha,\beta)}(\boldsymbol{r}) \mathrm{d}\Gamma + \int_{\Gamma_{l,Z}^{(\alpha,\beta)}} \tilde{p}^{(\alpha)}(\boldsymbol{r}) R_{l,Z}^{(\alpha,\beta)}(\boldsymbol{r}) \mathrm{d}\Gamma \right] = 0. \end{aligned} \tag{27}$$

Like in the Galerkin weighting procedure, used in the FEM, the weighting functions $\tilde{p}^{(\alpha)}$ are expanded in terms of the same set of basis functions used in the pressure expansions (14) and (21):

$$\tilde{p}^{(\alpha)}(\boldsymbol{r}) = \sum_{w=1}^{n_w^{(\alpha)}} \tilde{p}_w^{(\alpha)} \Phi_w^{(\alpha)}(\boldsymbol{r}) = \boldsymbol{\Phi}^{(\alpha)}(\boldsymbol{r}) \tilde{\boldsymbol{p}}_w^{(\alpha)}. \tag{28}$$

From here onwards, the position dependency of the vectors is omitted in the notations to enhance the readability.

Substitution of the pressure expansion (14) and the weighting function expansion (28) into the weighted residual formulation (27) yields a matrix equation linking the unknown wave function contributions for subdomain $\Omega^{(\alpha)}$ to those of the adjacent subdomains:

$$\tilde{\boldsymbol{p}}_{\boldsymbol{w}}^{(\alpha)T}[\boldsymbol{C}_{\boldsymbol{aa}}^{(\alpha,1)}\boldsymbol{p}_{\boldsymbol{w}}^{(1)}+\cdots+\boldsymbol{C}_{\boldsymbol{aa}}^{(\alpha,\alpha-1)}\boldsymbol{p}_{\boldsymbol{w}}^{(\alpha-1)}+\boldsymbol{A}_{\boldsymbol{aa}}^{(\alpha)}\boldsymbol{p}_{\boldsymbol{w}}^{(\alpha)}+\boldsymbol{C}_{\boldsymbol{aa}}^{(\alpha,\alpha+1)}\boldsymbol{p}_{\boldsymbol{w}}^{(\alpha+1)}+\cdots+\boldsymbol{C}_{\boldsymbol{aa}}^{(\alpha,N_\Omega+1)}\boldsymbol{p}_{\boldsymbol{w}}^{(N_\Omega+1)}-\boldsymbol{f}_{\boldsymbol{a}}^{(\alpha,1)}-\cdots-\boldsymbol{f}_{\boldsymbol{a}}^{(\alpha,\alpha-1)}-\boldsymbol{f}_{\boldsymbol{a}}^{(\alpha)}-\boldsymbol{f}_{\boldsymbol{a}}^{(\alpha,\alpha+1)}-\cdots-\boldsymbol{f}_{\boldsymbol{a}}^{(\alpha,N_\Omega+1)}]=0. \tag{29}$$

For a detailed description of integral formulations underlying the acoustic system matrices $\boldsymbol{A}_{\boldsymbol{aa}}^{(\bullet,\bullet)}$, coupling matrices $\boldsymbol{C}_{\boldsymbol{aa}}^{(\bullet,\bullet)}$ and loading vectors $\boldsymbol{f}_{\boldsymbol{a}}^{(\bullet)}$ the reader is referred to Pluymers [36]. Enforcing that this formulation holds for any weighting function requires the matrix equation between brackets to be zero.

Construction of a similar set of algebraic equations for all subdomains $\Omega^{(\alpha)}$, $\alpha = 1,\ldots,N_\Omega + 1$ and assembly of these results in a fully populated, complex and generally non-symmetric system of equations consisting of n_W algebraic equations governing the n_W unknown wave function contribution factors p_w:

$$\begin{bmatrix} \boldsymbol{A}_{\boldsymbol{aa}}^{(1,1)} & \boldsymbol{C}_{\boldsymbol{aa}}^{(1,2)} & \cdots & \boldsymbol{C}_{\boldsymbol{aa}}^{(1,N_\Omega+1)} \\ \boldsymbol{C}_{\boldsymbol{aa}}^{(2,1)} & \boldsymbol{A}_{\boldsymbol{aa}}^{(2,2)} & \cdots & \boldsymbol{C}_{\boldsymbol{aa}}^{(2,N_\Omega+1)} \\ \vdots & \vdots & \ddots & \vdots \\ \boldsymbol{C}_{\boldsymbol{aa}}^{(N_\Omega+1,1)} & \boldsymbol{C}_{\boldsymbol{aa}}^{(N_\Omega+1,2)} & \cdots & \boldsymbol{A}_{\boldsymbol{aa}}^{(N_\Omega+1,N_\Omega+1)} \end{bmatrix} \cdot \begin{bmatrix} \boldsymbol{p}_{\boldsymbol{w}}^{(1)} \\ \boldsymbol{p}_{\boldsymbol{w}}^{(2)} \\ \vdots \\ \boldsymbol{p}_{\boldsymbol{w}}^{(N_\Omega+1)} \end{bmatrix} = \begin{bmatrix} \boldsymbol{f}_{\boldsymbol{a}}^{(1)} \\ \boldsymbol{f}_{\boldsymbol{a}}^{(2)} \\ \vdots \\ \boldsymbol{f}_{\boldsymbol{a}}^{(N_\Omega+1)} \end{bmatrix}. \tag{30}$$

The calculation of the matrix coefficients involves integrations of highly oscillatory functions. Because the WB method, like any Trefftz based method, yields ill-conditioned system matrices [40,41], the numerical integrations must be performed carefully, making sure that a sufficiently high accuracy in determining the matrix coefficients is obtained. The small model sizes, combined with the method's high convergence rate [28], make it possible for the WBM to tackle problems at higher frequencies and at an affordable computational cost as compared to the element based methods.

3.4. Solution of the system of equations and postprocessing

After selection of a converging set of wave functions and construction of the WB model, the third step in the WB modelling process is the solution of the WB matrix equation (30) for the n_W wave function contribution factors p_w.

The final step is backsubstitution of the resulting wave function contribution factors into the pressure expansions (14), yielding an approximation $\hat{p}(\boldsymbol{r})$ of the acoustic pressure field. Derived acoustic variables, such as acoustic velocities, intensities and power distributions, can be easily obtained from the proposed wave function set $\boldsymbol{\Phi}_{\boldsymbol{w}}$ and the calculated contribution factors $\boldsymbol{p}_{\boldsymbol{w}}$.

- An approximation $\hat{\boldsymbol{v}}$ of the acoustic velocity vector field results from:

$$\hat{\boldsymbol{v}} = \frac{j}{\rho_0\omega}(\nabla\boldsymbol{\Phi}\boldsymbol{p}_{\boldsymbol{w}} + \nabla\hat{p}_q). \tag{31}$$

- An approximation $\widehat{\boldsymbol{I}}$ of the (active) acoustic intensity vector field results from:

$$\widehat{\boldsymbol{I}} = \frac{1}{2}\Re\left((\boldsymbol{\Phi}\boldsymbol{p}_{\boldsymbol{w}} + \hat{p}_q)\overline{\left(\frac{j}{\rho_0\omega}(\nabla\boldsymbol{\Phi}\boldsymbol{p}_{\boldsymbol{w}} + \nabla\hat{\boldsymbol{p}}_q)\right)}\right). \tag{32}$$

- An approximation $\widehat{W}$ of the (active) acoustic power through a surface S results from:

$$\widehat{W} = \iint_S \frac{1}{2}\Re\left((\boldsymbol{\Phi}\boldsymbol{p}_{\boldsymbol{w}} + \hat{p}_q)\overline{\left(\frac{j}{\rho_0\omega}(\nabla\boldsymbol{\Phi}\boldsymbol{p}_{\boldsymbol{w}} + \nabla\hat{p}_q)\right)}\right)\boldsymbol{n}\,\mathrm{d}S \tag{33}$$

with $\boldsymbol{n}$ the normal vector on S, $\Re(\bullet)$ the real part of a complex quantity and $\bar{\bullet}$ the complex conjugate operator.

Note that – in contrast to the polynomial shape functions used in conventional element based techniques – there is no additional loss of accuracy as compared to the primary field variables in the derived variables, since the derivatives of wave functions are wave functions themselves with an identical spatial resolution as the primary field approximation functions.

4. A multi-level modelling concept for multiple-scattering problems

The WBM approach described in Section 3 has proven to be an efficient deterministic modelling technique for the study of low- and mid-frequency two-dimensional acoustic scattering problems. The applied partitioning approach and the underlying geometrical convergence requirements however impose severe limitations to the applicability of the method for multiple-scattering problems with many well separated scatterers. This section discusses these limitations into more detail and proposes a solution in the form of a novel multi-level modelling concept. This approach is based on an alternative problem partitioning strategy and the application of the superposition principle for the description of the steady-state acoustic pressure field in the exterior problem region Ω^+.

4.1. WBM modelling limitations

The WBM has shown to be efficient in modelling 2D acoustic radiation problems [34]. However, when multiple acoustic scatterers are present and a direct domain subdivision strategy as presented in Section 3 is used, the method's efficiency tends to deteriorate. This loss of efficiency originates from two effects:

- *Relationship between number of DOFs and size of the truncation circle Γ_t*: When the different scatterers are well separated, a large truncation circle is needed in order to enclose the entire configuration. The definition of the wave functions used to model the sound propagation in the exterior region Ω^+ reveals an inverse proportionality between the radius of the truncation circle and the circumferential spatial resolution of the basis functions. Hence, the use of a larger artificial boundary, requires more unbounded wave functions in order to retain a comparable representation accuracy. In addition, a large bounded interior region is created which needs to be modelled using the bounded wave function expansions of type (15). Expressions (18) and (19) show that the spatial resolution of these functions is proportional to the overall dimensions of the region which is being modelled. Hence, if the scatterers become more separated, the number of basis functions required to model the interior region rises approximately proportional with the truncation radius. The resulting computational load to build the acoustic system matrices (which requires the numerical evaluation of n_W^2 highly oscillatory integrals) rapidly becomes prohibitively high. This effect is similar to the limitations seen in classical DtN formulations for element-based numerical methods, where the number of unknowns for 2D problems grows approximately proportional with the square of the overall domain dimensions.
- *Geometrical convergence requirements of the WBM*: The proposed wave function expansion to approximate the steady-state acoustic pressure field in a bounded subdomain requires each of the subdomains to be convex in order to ensure the convergence of the method towards the exact solution. Since all the scatterers need to be included within a single circle, a complex partitioning of the interior region Ω^- is often needed in order to satisfy this condition. This increase in subdomains is disadvantageous for the convergence rate of the method, since it introduces many additional acoustic interfaces along which continuity conditions need to be enforced. Moreover, some very common geometrical features cannot be dealt with at all. A typical example of this is the study of the acoustic behaviour of a two-dimensional scatterer which contains two or more circular obstacles. Since the region between two holes or between a hole and the artificial boundary Γ_t introduced by the WBM modelling process needs to be partitioned into convex subdomains, only an approximate, linearised representation of the circular edge can be used to construct a convergent WBM model. The resulting model is only a crude geometrical approximation of the actual problem and has the additional disadvantage of being inefficient since a reasonable representation accuracy of the circle requires many convex subdomains surrounding it.

4.2. Multiple-scattering problem decomposition

The limitations of the WBM for the analysis of multiple-scattering problems described above can be resolved if a composite truncation boundary Γ_t' is defined which consists of a collection of circles, each of which encloses one single scattering object. In contrast to the modelling approach detailed in Section 3, the exterior solution field $p^{N_\Omega+1}$ can no longer be expanded in terms of a single series of exact solutions of the Helmholtz equation since there exists no single coordinate system in which the Helmholtz operator is separable in the exterior domain Ω^+ which is associated with Γ_t'. Moreover, the solution field is no longer purely outgoing in Ω^+, since part of the scattered field leaving one of the circular boundaries may reenter another and vice versa.

Similar to Grote [23], the derivation of this approach starts by considering the general two-scatterer problem given in Fig. 3. In a first step, each of the scatterers $i = 1,2$ is enclosed by a close-fitting circular truncation boundary $\Gamma_{t,i}'$ and a local polar coordinate system (r_i,θ_i) is defined in the center c_i of these circles. We define the exterior regions outside of both truncations as $\Omega^{+,1}$ and $\Omega^{+,2}$. Based on these definitions, the exterior solution field $p^{N_\Omega+1}$ is now decomposed into two purely outgoing wave fields $p^{(N_\Omega+1,1)}$ and $p^{(N_\Omega+1,2)}$, which solve the Helmholtz equation and the Sommerfeld radiation condition in one of these regions:

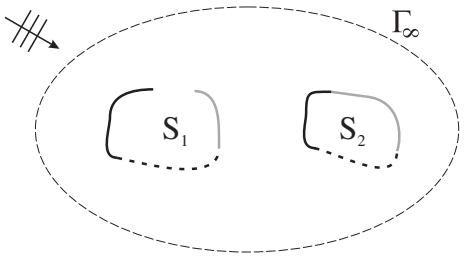

Fig. 3. General two scatterer problem.

$$\nabla p^{(N_\Omega+1,1)}(r_1,\theta_1)+k^2 p^{(N_\Omega+1,1)}(r_1,\theta_1)=0,\quad (r_1,\theta_1)\in\Omega^{+,1}, \tag{34}$$

$$\lim_{r\to\infty}\left(\sqrt{r}\left(\frac{\partial}{\partial r}+jk\right)p^{(N_\Omega+1,1)}\right)=0 \tag{35}$$

and

$$\nabla p^{(N_\Omega+1,2)}(r_2,\theta_2)+k^2 p^{(N_\Omega+1,2)}(r_2,\theta_2)=0,\quad (r_2,\theta_2)\in\Omega^{+,2}, \tag{36}$$

$$\lim_{r\to\infty}\left(\sqrt{r}\left(\frac{\partial}{\partial r}+jk\right)p^{N_{(\Omega}+1,2)}\right)=0. \tag{37}$$

Both fields are constructed independently of each other. Field $p^{(N_\Omega+1,1)}$ is entirely determined by the conditions which are imposed along the truncation circle $\Gamma'_{t,1}$ and field $p^{(N_\Omega+1,2)}$ only depends on the conditions along $\Gamma'_{t,2}$. To solve these problems, the WBM for unbounded problems as described in Section 3 can be applied. This results in two independent wave function expansions for each of the outgoing wave fields:

$$\Phi_n^{(N_\Omega+1,i)}(r_i,\theta_i)=\begin{cases}\Phi_{n_c}^{(N_\Omega+1,i)}(r_i,\theta_i)=H_n^{(2)}(kr_i)\cos(n\theta_i),\\ \Phi_{n_s}^{(N_\Omega+1,i)}(r_i,\theta_i)=H_n^{(2)}(kr_i)\sin(n\theta_i),\end{cases}\quad i=1,2. \tag{38}$$

Finally, the wave field of interest $p^{(N_\Omega+1)}$ is coupled to both outgoing wave fields $p^{(N_\Omega+1,1)}$ and $p^{(N_\Omega+1,2)}$ by matching $p^{(N_\Omega+1,1)}+p^{(N_\Omega+1,2)}$ to $p^{(N_\Omega+1)}$ along $\Gamma'_t=\Gamma'_{t,1}\cup\Gamma'_{t,2}$:

$$p^{(N_\Omega+1)}(r,\theta)=p^{(N_\Omega+1,1)}(r,\theta)+p^{(N_\Omega+1,2)}(r,\theta),\quad (r,\theta)\in\Gamma'_t. \tag{39}$$

Since the behaviour of both outgoing wavefields is entirely determined by their behaviour on Γ'_t, relationship (39) holds for the entire exterior region $\Omega^+=\Omega^{+,1}\cap\Omega^{+,2}$ of the originally proposed problem partitioning. For the proof of the existence and uniqueness of the proposed decomposition, the reader is referred to Grote [23].

4.3. A multi-level WBM modelling concept for multiple-scattering problems

The decomposition proposed above can be used as a basis for the so-called multi-level WBM modelling approach for the study of multiple-scattering problems. This approach is represented for a general two-scatterer problem in Fig. 4, but can easily be extended to a general configuration of n_λ scatterers. Each of the truncation circles $\Gamma'_{t,i}$, defines a 'level' L_i in the multiple scattering model, the outgoing wave-field in each of which can be described using a wave function expansion of type (38). By matching all these expansions, the pressure field in the exterior region Ω^+ of the total problem will be described as a summation of the fields present in each level:

$$p^{(N_\Omega+1)}=\sum_{L_i=1}^{n_\lambda}\boldsymbol{\Phi}^{(\boldsymbol{N}_\Omega+\mathbf{1},\boldsymbol{L}_i)}\cdot\boldsymbol{p}_{\boldsymbol{n}}^{(\boldsymbol{N}_\Omega+\mathbf{1},\boldsymbol{L}_i)}=[\boldsymbol{\Phi}^{(\boldsymbol{N}_\Omega+\mathbf{1},\boldsymbol{L}_1)}\cdots\boldsymbol{\Phi}^{(\boldsymbol{N}_\Omega+\mathbf{1},\boldsymbol{L}_{n_\lambda})}]\cdot\begin{bmatrix}\boldsymbol{p}_{\boldsymbol{n}}^{(\boldsymbol{N}_\Omega+\mathbf{1},\boldsymbol{L}_1)}\\ \vdots\\ \boldsymbol{p}_{\boldsymbol{n}}^{(\boldsymbol{N}_\Omega+\mathbf{1},\boldsymbol{L}_{n_\lambda})}\end{bmatrix}. \tag{40}$$

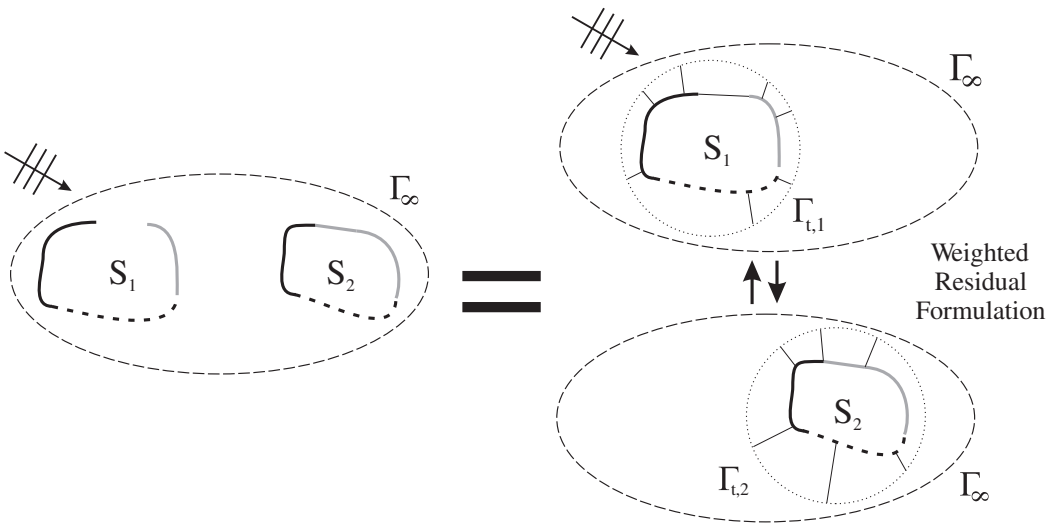

Fig. 4. The multi-level WBM modelling approach.

With the function set known, the wave model for this domain can now be constructed by enforcing the boundary and continuity conditions through the application of a weighted residual formulation. The residuals of the boundary conditions are again given by (24), now evaluated using the new, composite wave function set. The continuity conditions can be used to couple the multi-level unbounded wave set with bounded domains in the appropriate level, in the same way as a coupling would be set up between a conventional unbounded and bounded wave domain. The bounded domain in each of the levels can then further be modelled using the conventional wave based domain division techniques and function sets. The weighted residual formulation is written as:

$$
\begin{aligned}
&\sum_{\alpha=1}^{N_\Omega}\left(\int_{\Gamma_v^{(\alpha)}}\tilde{p}^{(\alpha)}(\boldsymbol{r})R_v^{(\alpha)}(\boldsymbol{r})\mathrm{d}\Gamma+\int_{\Gamma_Z^{(\alpha)}}\tilde{p}^{(\alpha)}(\boldsymbol{r})R_Z^{(\alpha)}(\boldsymbol{r})\mathrm{d}\Gamma+\int_{\Gamma_p^{(\alpha)}}-\mathcal{L}_v^{(\alpha)}(\tilde{p}^{(\alpha)}(\boldsymbol{r}))R_p^{(\alpha)}(\boldsymbol{r})d\Gamma+\sum_{\beta=1,\beta\neq\alpha}^{N_\Omega}\left[\int_{\Gamma_{l,p}^{(\alpha,\beta)}}-\mathcal{L}_v^{(\alpha)}(\tilde{p}^{(\alpha)}(\boldsymbol{r}))R_{l,p}^{(\alpha,\beta)}(\boldsymbol{r})\mathrm{d}\Gamma\right.\right.\\
&\left.+\int_{\Gamma_{l,v}^{(\alpha,\beta)}}\tilde{p}^{(\alpha)}(\boldsymbol{r})R_{l,v}^{(\alpha,\beta)}(\boldsymbol{r})\mathrm{d}\Gamma+\int_{\Gamma_{l,Z}^{(\alpha,\beta)}}\tilde{p}^{(\alpha)}(\boldsymbol{r})R_{l,Z}^{(\alpha,\beta)}(\boldsymbol{r})\mathrm{d}\Gamma\right]+\int_{\Gamma_{l,p}^{(\alpha,N_\Omega+1)}}-\mathcal{L}_v^{(\alpha)}(\tilde{p}^{(\alpha)}(\boldsymbol{r}))R_{l,p}^{(\alpha,N_\Omega+1)}(\boldsymbol{r})\mathrm{d}\Gamma\\
&+\int_{\Gamma_{l,v}^{(\alpha,N_\Omega+1)}}\tilde{p}^{(\alpha)}(\boldsymbol{r})R_{l,v}^{(\alpha,N_\Omega+1)}(\boldsymbol{r})\mathrm{d}\Gamma+\int_{\Gamma_{l,Z}^{(\alpha,N_\Omega+1)}}\tilde{p}^{(\alpha)}(\boldsymbol{r})R_{l,Z}^{(\alpha,N_\Omega+1)}(\boldsymbol{r})\mathrm{d}\Gamma\Bigg)\\
&+\sum_{L_i=1}^{n_\lambda}\left(\int_{\Gamma_v^{(N_\Omega+1,L_i)}}\tilde{p}^{(N_\Omega+1,L_i)}(\boldsymbol{r})R_v^{(N_\Omega+1)}(\boldsymbol{r})\mathrm{d}\Gamma+\int_{\Gamma_Z^{(N_\Omega+1,L_i)}}\tilde{p}^{(N_\Omega+1,L_i)}(\boldsymbol{r})R_Z^{(N_\Omega+1)}(\boldsymbol{r})\mathrm{d}\Gamma\right.\\
&+\int_{\Gamma_p^{(N_\Omega+1,L_i)}}-\mathcal{L}_v^{(N_\Omega+1)}(\tilde{p}^{(N_\Omega+1,L_i)}(\boldsymbol{r}))R_p^{(N_\Omega+1)}(\boldsymbol{r})d\Gamma+\sum_{\beta=1}^{N_\Omega}\left[\int_{\Gamma_{l,p}^{((N_\Omega+1,L_i),\beta)}}-\mathcal{L}_v^{(N_\Omega+1)}(\tilde{p}^{(N_\Omega+1,L_i)}(\boldsymbol{r}))R_{l,p}^{(N_\Omega+1,\beta)}(\boldsymbol{r})\mathrm{d}\Gamma\right.\\
&\left.\left.+\int_{\Gamma_{l,v}^{((N_\Omega+1,L_i),\beta)}}\tilde{p}^{(N_\Omega+1,L_i)}(\boldsymbol{r})R_{l,v}^{(N_\Omega+1,\beta)}(\boldsymbol{r})\mathrm{d}\Gamma+\int_{\Gamma_{l,Z}^{((N_\Omega+1,L_i),\beta)}}\tilde{p}^{(N_\Omega+1,L_i)}(\boldsymbol{r})R_{l,Z}^{(N_\Omega+1,\beta)}(\boldsymbol{r})\mathrm{d}\Gamma\right]\right)=0
\end{aligned}
\tag{41}
$$

with $\Gamma_\bullet^{(N_\Omega+1,L_i)}=\Gamma_\bullet^{(N_\Omega+1)}\bigcap\Gamma'_{t,L_i}$ and $\Gamma_{l,\bullet}^{((N_\Omega+1,L_i),\beta)}=\Gamma_{l,\bullet}^{(N_\Omega+1,\beta)}\bigcap\Gamma'_{t,L_i}$.

By enforcing the weighted residual formulation (41), the residuals on the imposed boundary and continuity conditions are minimised in an integral sense with respect to a set of weighting functions $\tilde{p}^{(\bullet)}(\boldsymbol{r})$. If these weighting functions are chosen to be any arbitrary function, enforcing the integral equation will minimise the residual errors themselves. To obtain a numerical model which can be solved, the test functions need to be expanded in terms of a limited set of basis functions $t_w(\boldsymbol{r})$:

$$
\tilde{p}^{(\bullet)}(\boldsymbol{r})=\sum_{a=1}^{n_w^{(\bullet)}}\tilde{p}_w^{(\bullet)}t_w^{(\bullet)}(\boldsymbol{r})=\boldsymbol{t}^{(\bullet)}(\boldsymbol{r})\tilde{\boldsymbol{p}}_{\boldsymbol{w}}^{(\bullet)},
\tag{42}
$$

In order to minimise the residual errors along the boundaries and interfaces, a complete set of basis functions $t_w(\boldsymbol{r})$ must be used to expand the weighting functions. The choice of basis functions may vary for each boundary but needs to be able to represent any arbitrary field on the associated boundary. In a conventional WBM domain, the entire set of basis functions used to approximate the acoustic pressure field inside the domain is used as weighting functions, following the classical Galerkin weighted residual approach. In the case of a multi-level WBM model however, the use of the full basis for the pressure field in the external region is unnecessary since the unbounded basis functions $\Phi_n^{N_\Omega+1,Li}$ are chosen such that they can accurately approximate any field on the associated truncation circle $\Gamma'_{t,Li}$. The addition of functions of the remaining truncation circles introduces unneeded information to the expansion and results in a deterioration of the already unfavourable numerical conditioning of the WBM system of equations. The choice of basis functions to expand the weighting functions in the resulting multi-level WBM model can be summarised as:

$$
t_w(\mathbf{r})=\begin{cases}\Phi_w^{(\alpha)}(\mathbf{r}) & \mathbf{r}\in\partial\Omega^{(\alpha)},\\ \Phi_w^{(N_\Omega+1,L_i)}(\mathbf{r}) & \mathbf{r}\in\Gamma'_{t,L_i}.\end{cases}
\tag{43}
$$

5. Numerical validation

In this section the applicability and efficiency of the proposed modelling approach is validated based on three numerical validation studies, which have an increasing level of modelling complexity. First, the accuracy and convergence of the method is assessed based on the study of the scattering behaviour of a single circular scatterer which can be sound-hard (zero normal velocity) or sound-soft (zero acoustic pressure). Next, the feasibility of the approach is shown based on the scattering behaviour of a configuration of five circular scatterers in air on which different combinations of acoustic boundary conditions are applied. Finally, the efficiency of the method is illustrated by means of a general underwater acoustics problem, in which five complex shaped scatterers are present. A generic Matlab implementation of both the classical and multi-level WBM approach is used in this validation study.

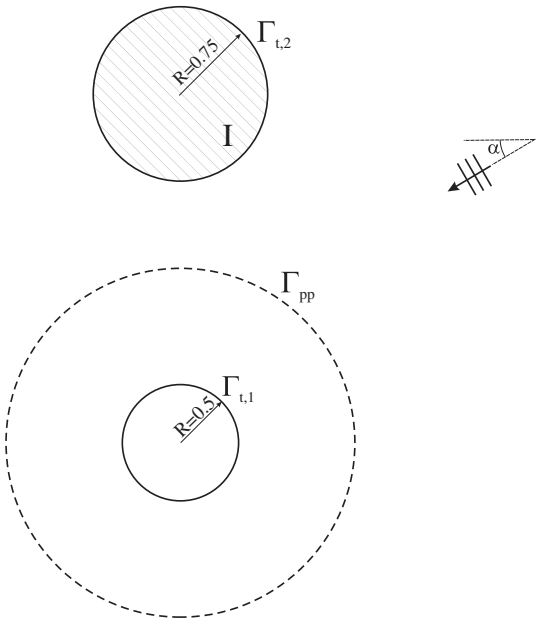

Fig. 5. Validation example 1: problem definition.

5.1. Accuracy and convergence assessment: single-scattering problem

In order to assess the accuracy and convergence of the proposed methodology we consider the simple single-scatterer problem given in Fig. 5. A plane wave which propagates in air (c = 340 m/s, ρ_0 = 1.225 kg/m^3) at an angle of incidence α impinges on a single circular scatterer. This scatterer is centered at point $c_1 = (0,0)$ and has a radius of 0.5m. On the surface of this obstacle both uniform sound-soft and uniform sound-hard boundary conditions are considered. In this way, the Anger–Jacobi series expansion [42] can be used to obtain an exact reference solution $p_{ref}(\boldsymbol{r})$ for the scattered field. Both problems can be modelled efficiently using the classical WBM approach. This requires the definition of a truncation boundary Γ_t which coincides with the scatterer boundary along which the required boundary conditions are applied. In order to validate the multi-level extension of the WBM, a second circular truncation $\Gamma'_{t,2}$ is introduced. This boundary is centered at $c_2 = (0,3)$ and has a radius of 0.75 m. The entire region enclosed by $\Gamma'_{t,2}$ is filled with a single bounded WBM subdomain which is coupled to the exterior region using the equivalent normal velocity coupling conditions with the characteristic impedance $\rho_0 c$ as coupling impedance $\overline{Z}_{int}$. The number of wave functions in the interior domain is chosen such that the spatial resolution of the interior expansion matches that of the exterior pressure expansion along the interface $\Gamma'_{t,2}$. In this way, the incident and scattered fields are simply transmitted through the domain and the second scatterer becomes acoustically transparent.

The predicted acoustic pressure field at 2040 Hz using the multi-level WBM model which applies an expansion (38) using N = 50 circumferential orders for the approximation for the unbounded pressure $p^{(N_\Omega+1,i)},\ i = 1,2$ is compared to an exact solution calculated in a region which contains both the actual scatterer and the artificial scattering level. At this frequency, the product of the acoustic wavenumber k and a problem related dimension a, being the radius of the scatterer, equals $ka = 6\pi$. In Fig. 6(a), the real part of the acoustic field due to a plane wave which impinges at an angle of incidence $\alpha = \pi/3$ on a sound-soft scatterer is shown. This figure shows that the resulting pressure field is continuous across the artificial boundary $\Gamma'_{t,2}$, which is indicated by the dashed circle. The accuracy of the multiple-scattering model is given in more detail in Fig. 6(b), which shows the relative prediction errors ε as defined by Eq. (44) for multi-level WBM predictions of the complex amplitude of the resulting pressure field with respect to the exact solution. The distribution of ε shows that the largest approximation errors occur on the artificial truncation boundary but they are still less than 10^{-5}. The overall prediction accuracy in the rest of the computational domain is however not influenced by these errors and a nearly perfect match with the analytical solution is observed.

$$\varepsilon(\hat{p}(\boldsymbol{r})) = \frac{|\hat{p}(\boldsymbol{r}) - p_{ref}(\boldsymbol{r})|}{|p_{ref}(\boldsymbol{r})|} \tag{44}$$

The accuracy of the multi-level modelling approach is studied in more detail by computing the scattered acoustic field for several combinations of possible values for the excitation frequency, the angle of incidence α, the scatterer boundary conditions and the number of orders N used in the WBM approximation. In Table 1, the average relative prediction error for the complex acoustic pressure amplitude ε_{av} as defined by Eq. (45) in N_{pp} = 2500 points on a postprocessing circle Γ_{pp} which encircles the acoustic scatterer are given for a total of 24 possible problem definitions (two types of boundary conditions,

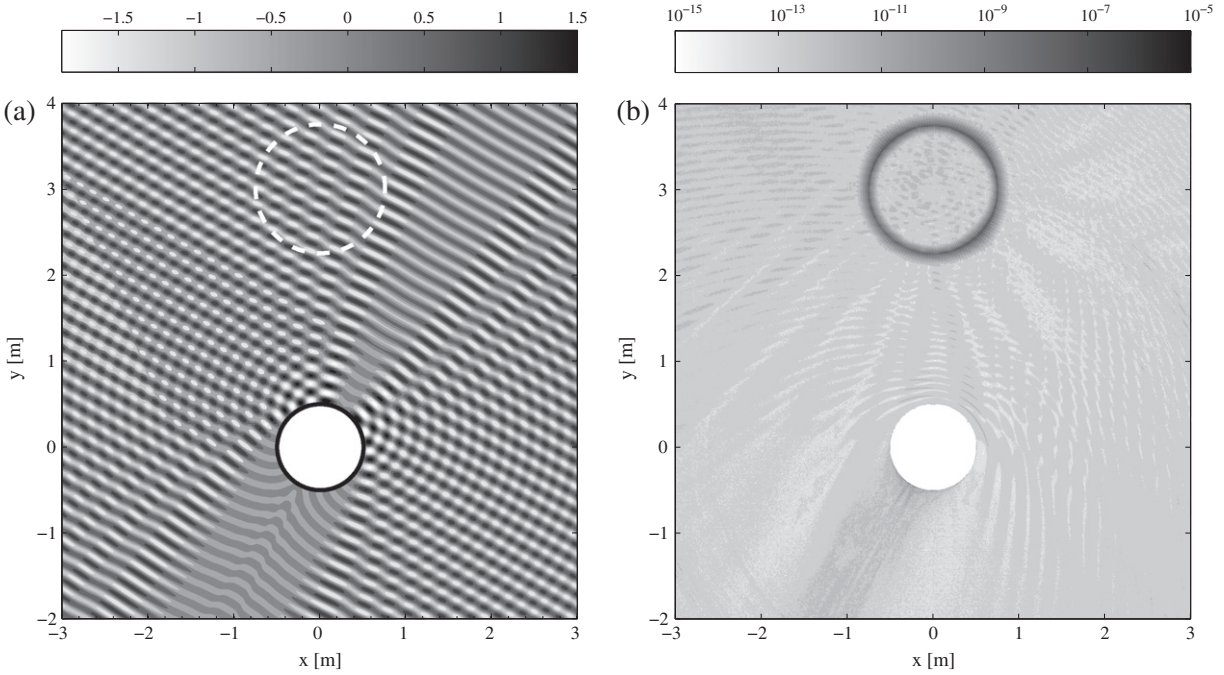

Fig. 6. Validation example 1: contour plots, $ka = 6\pi$, $N = 50$, $\alpha = \pi/6$, sound-soft boundary conditions: (a) $\Re(\hat{p}(\boldsymbol{r}))$ (Pa), (b) Relative prediction errors ε (–).

Table 1
Validation example 1: average prediction accuracy ε_{av} compared to an exact solution for the plane wave scattering of a single circular scatterer along a circle with radius $R_{pp} = 1.5$ m.

α	$ka = 4\pi$		$ka = 6\pi$		$ka = 8\pi$	
	30	50	30	50	30	50
Sound-hard scatterer						
0	5.57×10^{-12}	1.64×10^{-14}	1.27×10^{-10}	6.92×10^{-15}	6.97×10^{-5}	1.59×10^{-14}
$\pi/6$	2.56×10^{-12}	9.57×10^{-15}	1.46×10^{-10}	1.31×10^{-14}	6.97×10^{-5}	1.37×10^{-14}
$\pi/3$	7.15×10^{-12}	1.46×10^{-14}	1.42×10^{-10}	1.27×10^{-14}	6.97×10^{-5}	1.01×10^{-14}
$\pi/2$	9.28×10^{-12}	1.10×10^{-14}	1.38×10^{-10}	5.90×10^{-15}	6.97×10^{-5}	1.15×10^{-14}
Sound-soft scatterer						
0	9.21×10^{-12}	2.04×10^{-14}	1.83×10^{-10}	1.07×10^{-14}	9.25×10^{-5}	2.93×10^{-14}
$\pi/6$	2.81×10^{-12}	1.47×10^{-14}	1.93×10^{-10}	2.12×10^{-14}	9.25×10^{-5}	2.19×10^{-14}
$\pi/3$	7.24×10^{-12}	2.24×10^{-14}	2.03×10^{-10}	1.62×10^{-14}	9.25×10^{-5}	1.56×10^{-14}
$\pi/2$	1.14×10^{-11}	1.00×10^{-14}	1.94×10^{-10}	1.04×10^{-14}	9.25×10^{-5}	1.41×10^{-14}

four possible angles of incidence and three excitation frequencies). All these problems are modelled using multi-level WBM models with two possible numbers of basis function orders for the exterior acoustic pressure fields linked to both modelling levels. The number of basis functions in the bounded subdomain is chosen such that the spatial resolution of the interior pressure expansion matches that of the unbounded wave functions. The errors show that the prediction accuracy is approximately independent of the angle of incidence and the imposed boundary conditions for a fixed number of orders in the expansion. All the models with 50 orders in the expansions for both levels have converged to the exact solution. The models with 30 orders show a decrease in prediction accuracy when the excitation frequency becomes higher. This can be explained by the fact that the circumferential spatial resolution of the wave functions in the unbounded pressure expansions is independent of the excitation frequency, while the acoustic wavelengths in the exact solution become shorter when the excitation frequency rises. As a result, more unbounded wave functions are needed to obtain a certain prediction accuracy.

$$\varepsilon_{av}(\hat{p}(\boldsymbol{r})) = \frac{1}{N_{pp}} \sum_{i=1}^{N_{pp}} \frac{|\hat{p}(\boldsymbol{r_i}) - p_{ref}(\boldsymbol{r_i})|}{|p_{ref}(\boldsymbol{r_i})|} \tag{45}$$

To study the effect of the number of orders N in the unbounded wave function expansion on the average acoustic pressure amplitude prediction error, Fig. 7 shows these errors for both the classical and multi-level WBM approach with varying N for

a sound-soft scattering problem with incidence angle $\alpha = \pi/6$ at $ka = 6\pi$ and a sound-hard scattering problem with $\alpha = \pi/12$ at $ka = 8\pi$. Both convergence curves show that for problems which can be handled with both approaches, the classical WBM and its multi-level expansion exhibit a very similar convergence behaviour and converge to the exact solution given by the analytical series expansion. These curves also illustrate the need for a higher number of basis functions in the unbounded wave function expansion to obtain a similar prediction accuracy at a higher excitation frequency.

5.2. Multiple-scattering problem: five circular obstacles

In this validation example, the scattering behaviour of a configuration of multiple circular shaped scatterers is considered. The aim of this study is to illustrate the applicability of the multi-level modelling strategy for multiple-scattering problems with arbitrary boundary conditions. The problem geometry is shown in Fig. 8. An acoustic plane wave propagates in air with

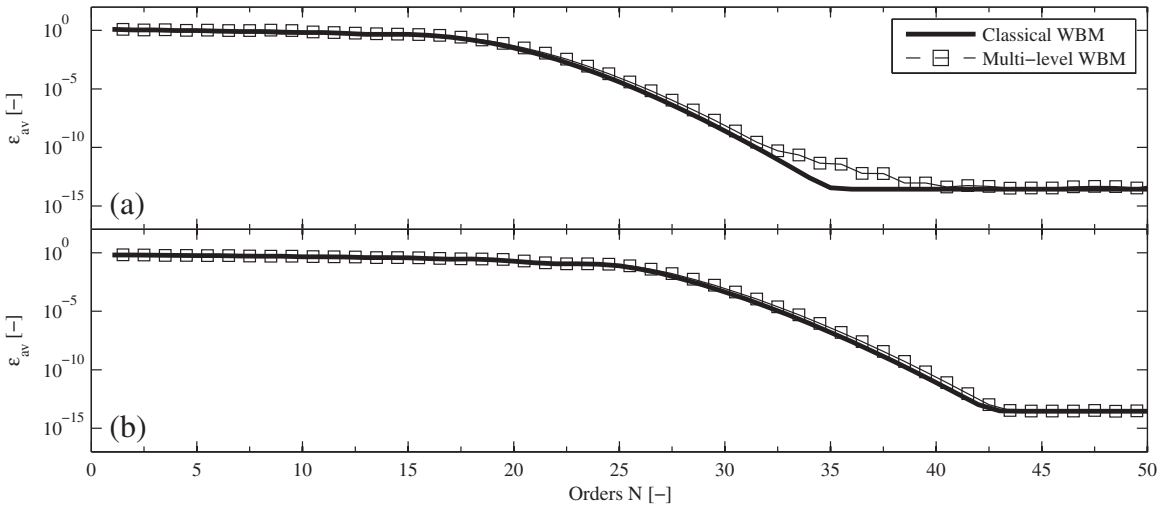

Fig. 7. Validation example 1: average relative prediction error ε_{av} as a function of the maximum order N in the function expansion for $\Gamma'_{t,1}$: (a) $ka = 6\pi$, $\alpha = \pi/6$, sound-soft boundary conditions, (b) $ka = 8\pi$, $\alpha = \pi/12$, sound-hard boundary conditions.

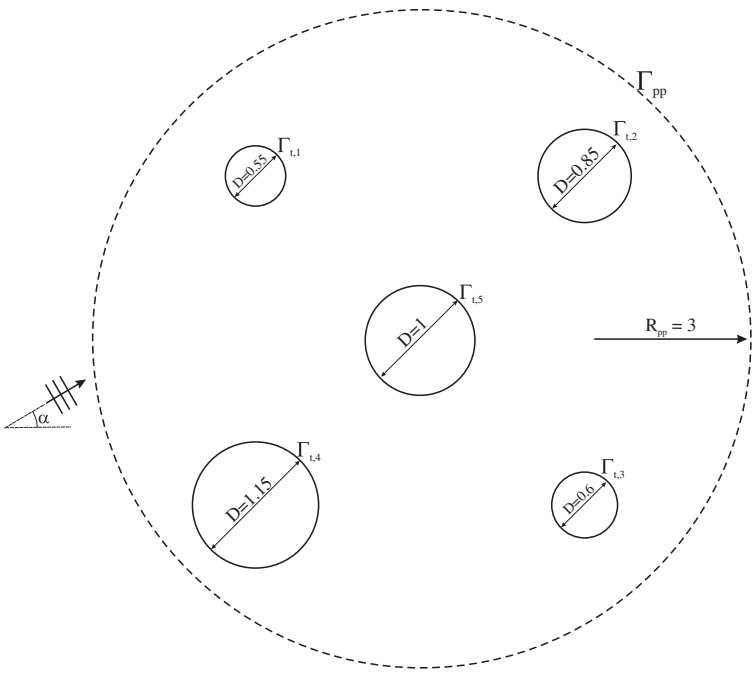

Fig. 8. Validation example 2: problem definition.

an incidence angle α and impinges on five circular obstacles with varying diameters ranging between 0.55 m and 1.15 m. The five scatterers are centered at the four corners and the centerpoint of a square with width and height 3 m. To study the behaviour of the proposed methodology at different frequencies, angles of incidence and with various types of boundary conditions, three problem settings are considered. Firstly, a collection of sound-hard scatterers on which a plane wave at $\alpha = \pi/8$ impinges is studied at $ka = 2\pi$, with a the radius of the largest scatterer. Secondly, all the surfaces are assumed to be sound-soft at $ka = 3\pi$ and $\alpha = \pi/4$. Finally, a constant acoustic impedance of $441 - 1241j$ Ns/m^3 is imposed on four of the five scatterers (modelled using truncation boundaries Γ_i', $i = 1, \ldots, 4$), while the central obstacle is sound-hard. This configuration is excited at $ka = 4\pi$ by a plane wave propagating at $\alpha = 3\pi/8$. Since no analytical solutions for these three problems exist, a refined indirect variational Boundary Element model (using 52,160 DOFs) is used to validate the results obtained with the multi-level WBM model consisting of five modelling levels.

In Fig. 9(a), the real part of the multi-level WBM acoustic pressure field for the second problem setting (sound-soft scatterers) is shown. In the multi-level model, a total of $N = 30$ orders is used to capture the circumferential variations in the pressure field on the largest scatterer Γ_1'. The number of orders used in the other modelling levels is chosen such that their spatial resolution matches that of the basis functions for Γ_1'. This results in a lower number of basis functions in the total model compared to the use of a fixed number of orders for the expansions for each of the modelling levels like in the first validation example and significantly reduces the computational effort for the multi-level WBM calculations. The figure shows that the imposed boundary conditions are accurately taken into account. The accuracy of the multiple-scattering model is given in more detail in Fig. 9(b), which shows the relative prediction errors ε (44) of the multi-level WBM prediction with respect to the BEM reference solution. The distribution of ε shows that the largest approximation errors occur in the shadow zone behind the scatterers. These errors originate from the low pressure values at these locations, which result in an inaccurate assessment of the relative prediction errors. The overall prediction accuracy in the whole computational domain shows a very good agreement between both models and is of the same order of magnitude as the accuracy of the BEM reference model.

Fig. 10 compares the real and imaginary parts of the predicted acoustic pressure fields along the circle Γ_{pp} with radius $R_{pp} = 3$ m with the BEM results for the scattered acoustic field for the three considered problem definitions. For all the quantities shown in this figure, a good agreement between both approaches is observed. These results indicate the applicability of the proposed approach for the study of multiple-scattering problems with general boundary conditions and show that the method is capable of tackling these problems at various frequencies and angles of incidence. These observations are further illustrated by the results presented in Table 2. In this table the influence of the number of approximation functions in the various levels of the WBM model and the excitation frequency on the averaged prediction accuracy ε_{av} (45) of the complex acoustic pressure amplitude in $N_{pp} = 2500$ points on Γ_{pp} becomes apparent. For each of the problem settings, four multi-level WBM models are built and solved. The first three apply respectively 20, 25 or 30 approximation function orders along the

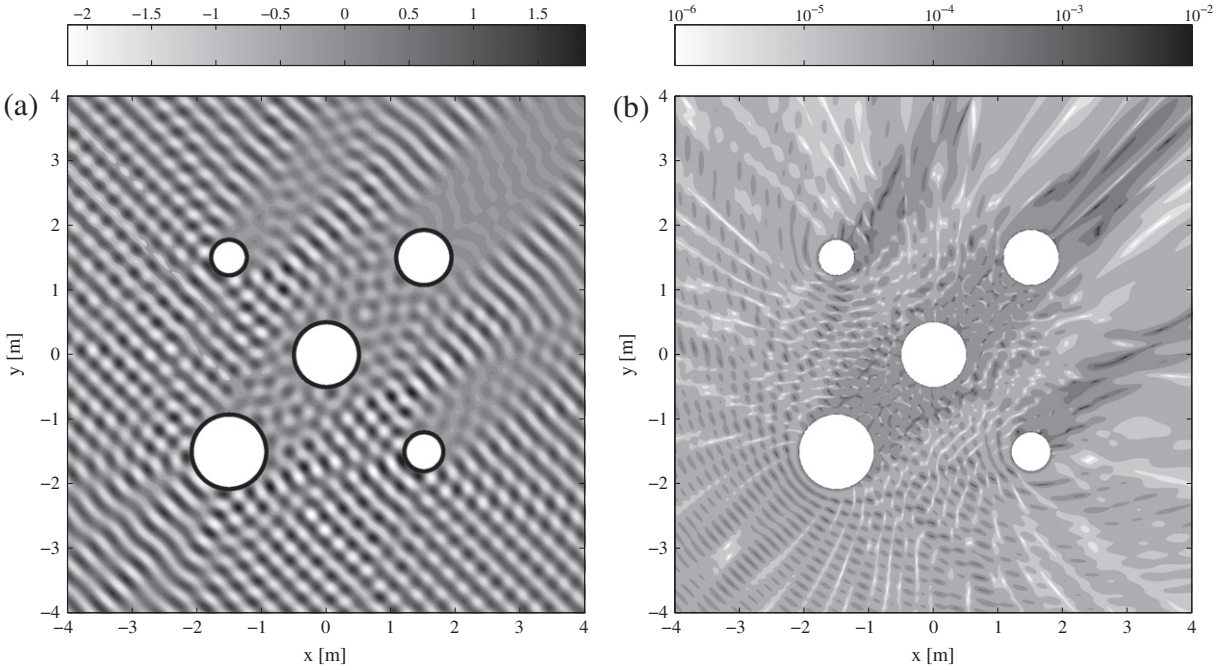

Fig. 9. Validation example 2: contour plots, $ka = 3\pi$, $N = 30$ on the largest scatterer, $\alpha = \pi/4$, sound-soft boundary conditions: (a) $\Re(\hat{p}(\boldsymbol{r}))$ (Pa), (b) Relative prediction errors ε (–).

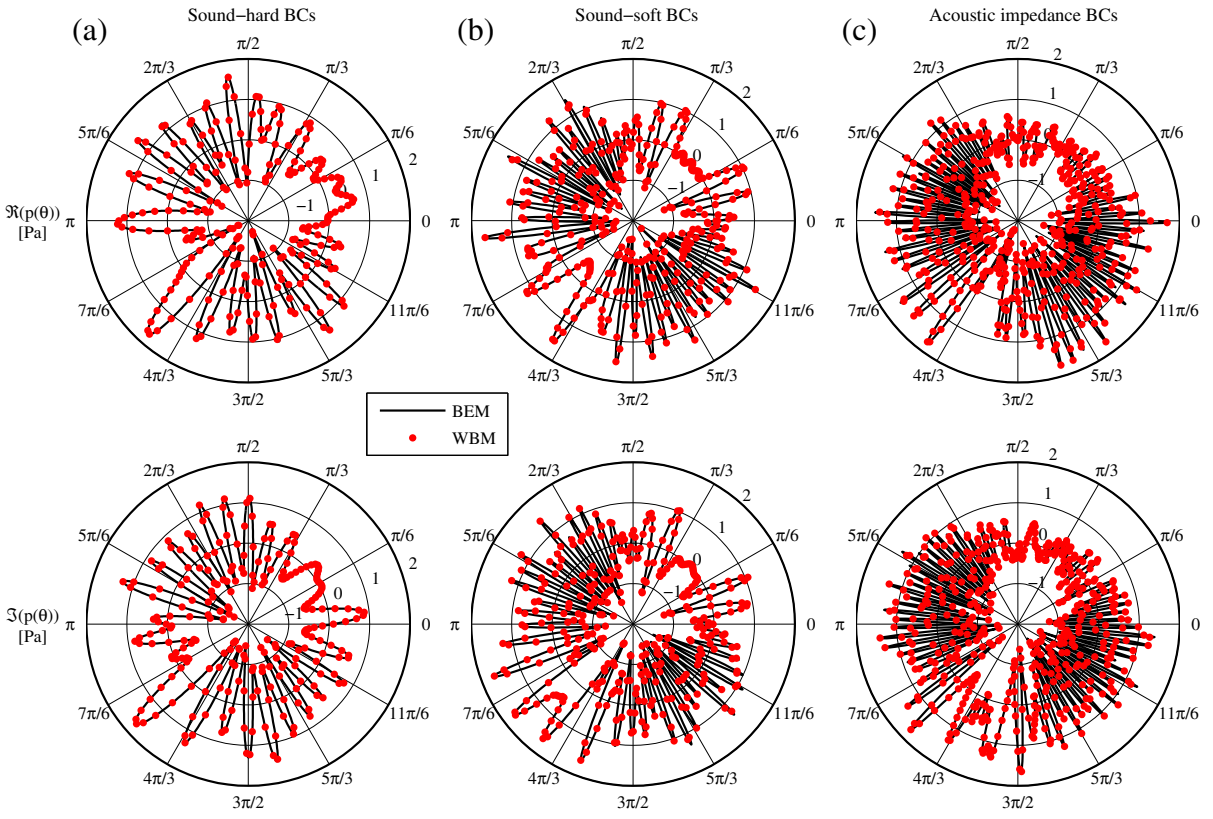

Fig. 10. Validation example 2: acoustic pressure values along a circle with radius $R_{pp} = 3m$: (a) $ka = 2\pi$, $N = 30$, $\alpha = \pi/8$, sound-hard boundary conditions, (b) $ka = 3\pi$, $N = 30$, $\alpha = \pi/4$, sound-soft boundary conditions, (c) $ka = 4\pi$, $N = 30$, $\alpha = 3\pi/8$, acoustic impedance boundary conditions.

Table 2
Validation example 2: average prediction accuracy ε_{av} compared to a reference BEM solution for the plane wave scattering of multiple circular scatterers along a circle with radius $R_{pp} = 3$ m.

N	*Orders*	♯ DOF$_{Li}$					♯ DOF$_{total}$	ε_{av} (−)
		L_1	L_2	L_3	L_4	L_5		
Sound-hard scatterers, $ka = 2\pi$, $a = \pi/8$								
20	Variable	41	21	35	19	29	145	4.79×10^{-5}
25	Variable	51	27	43	23	37	181	4.79×10^{-5}
30	Variable	61	31	53	29	45	219	4.79×10^{-5}
30	Constant	61	61	61	61	61	305	4.79×10^{-5}
Sound-soft scatterers, $ka = 4\pi$, $a = \pi/4$								
20	Variable	41	21	35	19	29	145	3.03×10^{-4}
25	Variable	51	27	43	23	37	181	9.58×10^{-5}
30	Variable	61	31	53	29	45	219	9.57×10^{-5}
30	Constant	61	61	61	61	61	305	9.57×10^{-5}
Damped scatterers, $ka = 6\pi$, $a = 3\pi/8$								
20	Variable	41	21	35	19	29	145	2.77×10^{-1}
25	Variable	51	27	43	23	37	181	7.70×10^{-3}
30	Variable	61	31	53	29	45	219	1.17×10^{-4}
30	Constant	61	61	61	61	61	305	1.17×10^{-4}

largest scattering boundary. The number of orders for the four other scatterers is chosen to match the spatial resolution of the I_1', as described above. The fourth model uses 30 orders for each of the pressure expansions in the exterior region. For the first problem setting, using 20 orders in the pressure expansion is sufficient for the WBM model to obtain the prediction accuracy of the reference BEM model. When the model is further refined, the average prediction accuracy remains the same. The sound-soft configuration shows that the model using 20 orders has not yet completely converged, but the other three models converge to the same accuracy, which is slightly higher than the final accuracy for the sound-hard case due to the

higher excitation frequency. For the acoustically damped problem, the prediction accuracy steadily increases when adding more basis functions until convergence is attained using 30 orders. The models using a constant number of orders result for each of the problem settings in exactly the same prediction accuracy as the models using a variable number of approximation functions for each of the scatterers, while the latter results in a model with 30% less degrees of freedom.

5.3. Performance assessment: complex multiple-scattering problem

Finally, the computational efficiency of the multi-level WBM approach for general acoustic multiple-scattering problems is studied by considering the example shown in Fig. 11. An acoustic point source is located inside a C-shape with a finite thickness. The resulting acoustic pressure field impinges on a configuration of four acoustic scatterers, two circles and two squares. All the scattering objects in this validation example are considered to be sound-hard. The acoustic medium surrounding the obstacles is water ($c = 1500$ m/s, $\rho_0 = 1000$ kg/m^3). The scattering behaviour of this configuration is studied in the frequency range between 50 Hz and 10,000 Hz ($ka \approx 0.1\pi \cdots 20\pi$, with $a = 1$, the outer radius of the C-shaped scatterer).

The underwater scattering problem is modelled using both the classical indirect variational BEM and the newly developed multi-level WBM modelling approach. Several BE models are built for this problem. The details of the models which are used in this validation study are listed in Table 3. For each of the models the number of degrees of freedom, the expected model validity and the computational load needed to calculate a pressure amplitude response function consisting of 996 frequency lines between 50 Hz and 10,000 Hz is given. The validity of the models is estimated using both a commonly applied rule of thumb, which states that at least six linear elements are needed to model a single acoustic wavelength, and a more complex rule derived in [25], taking into account numerical pollution effects which become dominant in the mid-frequency range. In the WBM models, a 5-level unbounded multi-level model is combined with 10 interior WBM subdomains. For the circular scatterers, the truncation boundaries of the associated WBM levels coincide with the scatterer geometry. The squares are modelled by taking a truncation circle which intersects the four corners and by introducing four disjoint bounded subdomains along each of the straight edges. The C-shape is modelled using a truncation circle which coincides with the outer circular edge of the C and adding two convex subdomains in the interior of the C. Along all the interfaces between the different subdomains in this model the pressure–velocity continuity conditions (8) and (9) are enforced. The total number of basis functions used in the WBM model is constant over the entire frequency range and is chosen such that the

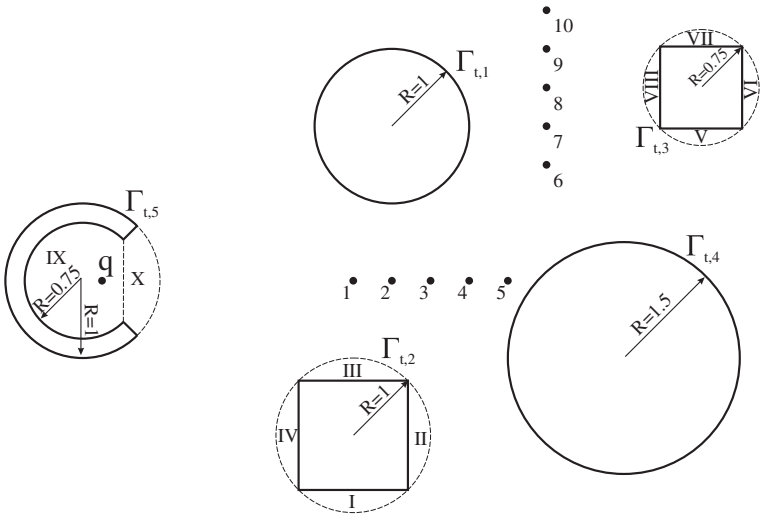

Fig. 11. Validation example 3: problem definition.

Table 3
Model information for validation example 3.

Element size (mm)	♯ DOF	Mesh validity: 6 el./λ (Hz)	Mesh validity [23] (Hz)	Calculation time (s)	ε_{av} (–)
Boundary Element Method					
11.5	5974	20,759.3	4685.7	7958.04	0.1044
3.0	22,902	79,577.5	11,477.1	334,357.20	0.0064
1.5	45,808	159,154.9	18,218.7	2,540,118.72	
Wave Based Method					
–	2153	–	–	8426.55	0.0065

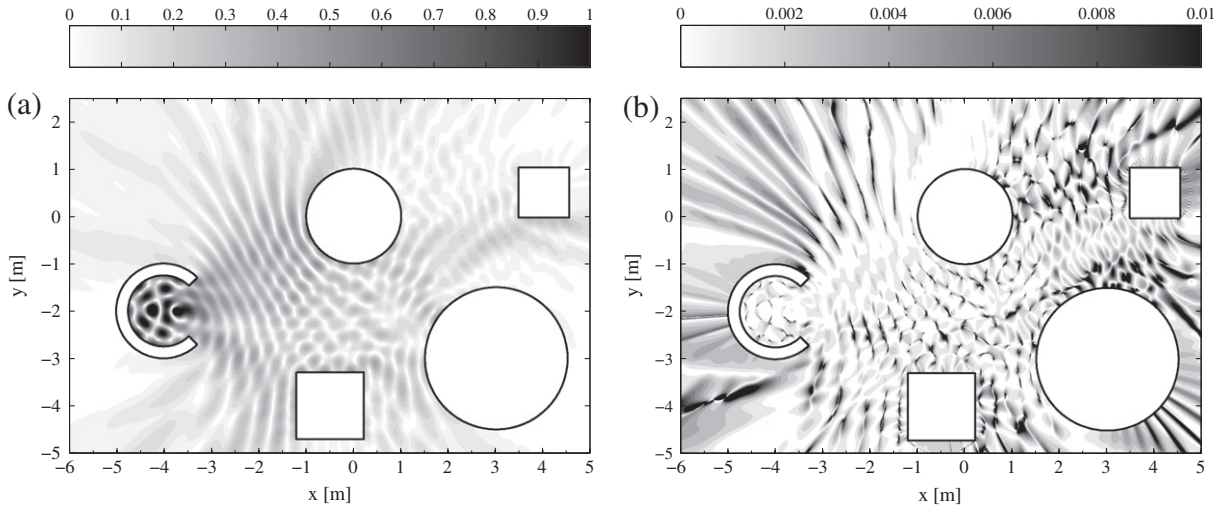

Fig. 12. Validation example 3: acoustic pressure contours at 3000 Hz ($ka = 6\pi$): (a) pressure amplitude (Pa), (b) relative pressure prediction errors ε (–).

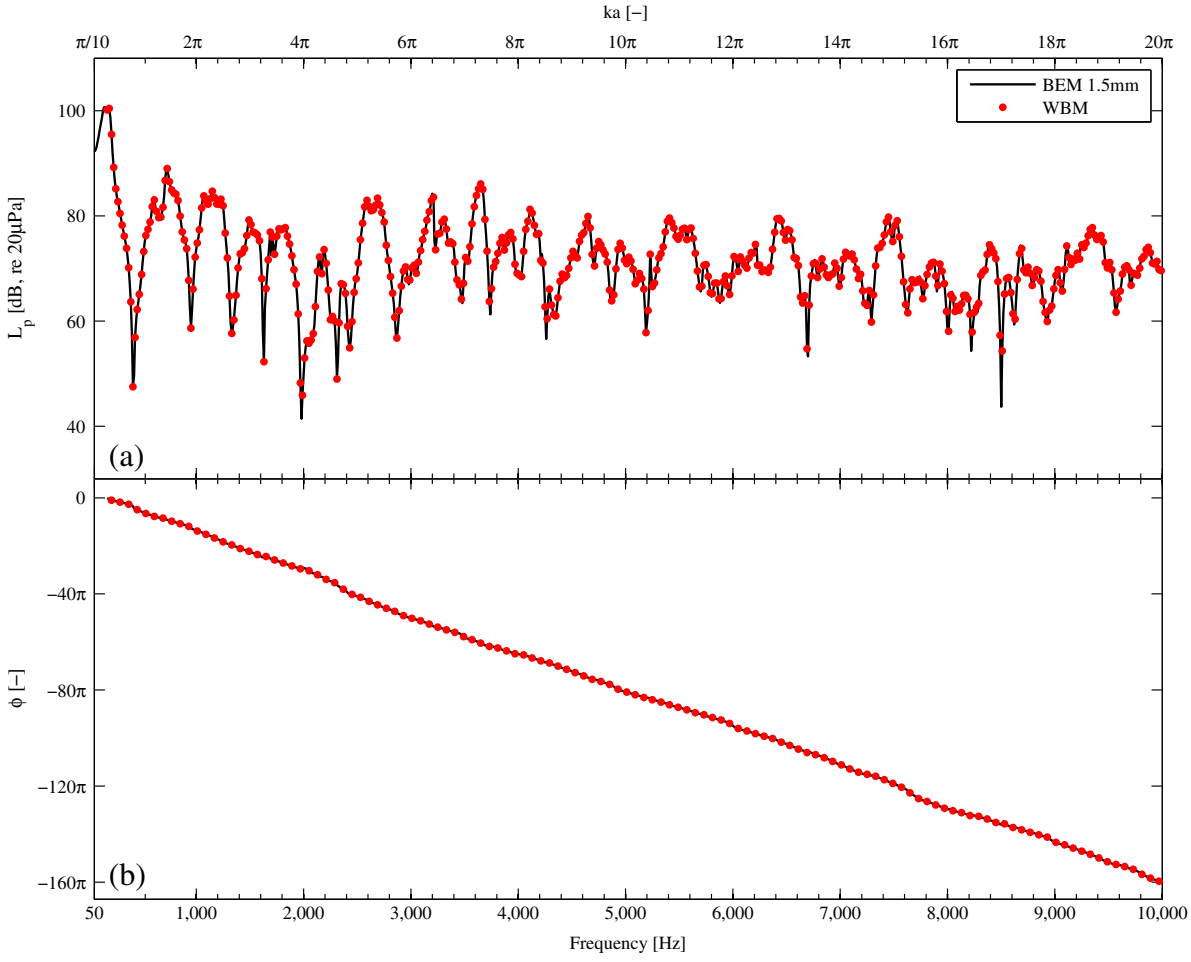

Fig. 13. Validation example 3: acoustic pressure response functions in response point 6: (a) sound pressure level L_p (dB, *re*20 μPa), (b) phase angle ϕ (–).

computational load of the model is approximately the same as that of the coarsest BEM model. The calculation times listed in this table consist of the cost of frequency-dependent operations only, being the time needed to build and solve the linear system of equations for the BEM and the time to build and solve the multi-level system matrices for the WBM. The multi-level WBM models are implemented using Matlab R2007b, while the BEM calculations are performed using LMS/Sysnoise5.6. All the calculations were carried out on a Linux based 2.66 GHz Intel Xeon system with 32 gigabytes of memory.

The contours in Fig. 12(a) show the amplitude of the acoustic pressure at 3000 Hz ($ka = 6\pi$), calculated using the multi-level WBM. In Fig. 12(b), the relative error ε (44) of this wave field with respect to the results from the reference BEM model ($h \approx 1.5$ mm) is shown. The acoustic amplitude prediction errors remain well within the range of 0–1%, except at the pressure nodal lines, where the error calculation itself is inaccurate due to almost-zero division.

Fig. 13 compares the frequency response function in the frequency range between 50 and 10,000 Hz of the acoustic sound pressure level L_p (46) and phase angle ϕ of the acoustic field in the response point 6 indicated in Fig. 11 for the BEM reference model and the multi-level WBM model. The good agreement between the WBM results and the reference is evident from this figure.

$$L_p = 20log_{10}\left(\frac{|\hat{p}(\boldsymbol{r})|}{20\ \mu\text{Pa}}\right) \tag{46}$$

A more detailed comparison is made in Fig. 14 where the frequency-dependent average pressure amplitude errors in the 10 response points in Fig. 11 for the two BEM models and the WBM model are shown. As shown in the bottom figure, the WBM model is valid over the entire frequency range presented here. It is clear that the WBM result (bottom figure) is far more accurate than the one obtained by the BEM model with the same calculation time (top figure). According to the commonly applied rule of thumb, the BEM model should be valid in the entire frequency range studied in this validation. The results however show that the prediction accuracy starts to deteriorate much earlier. The alternative validity criterion predicts this breakdown much more accurately. As shown in the middle figure, the BEM mesh needs to be refined in order to

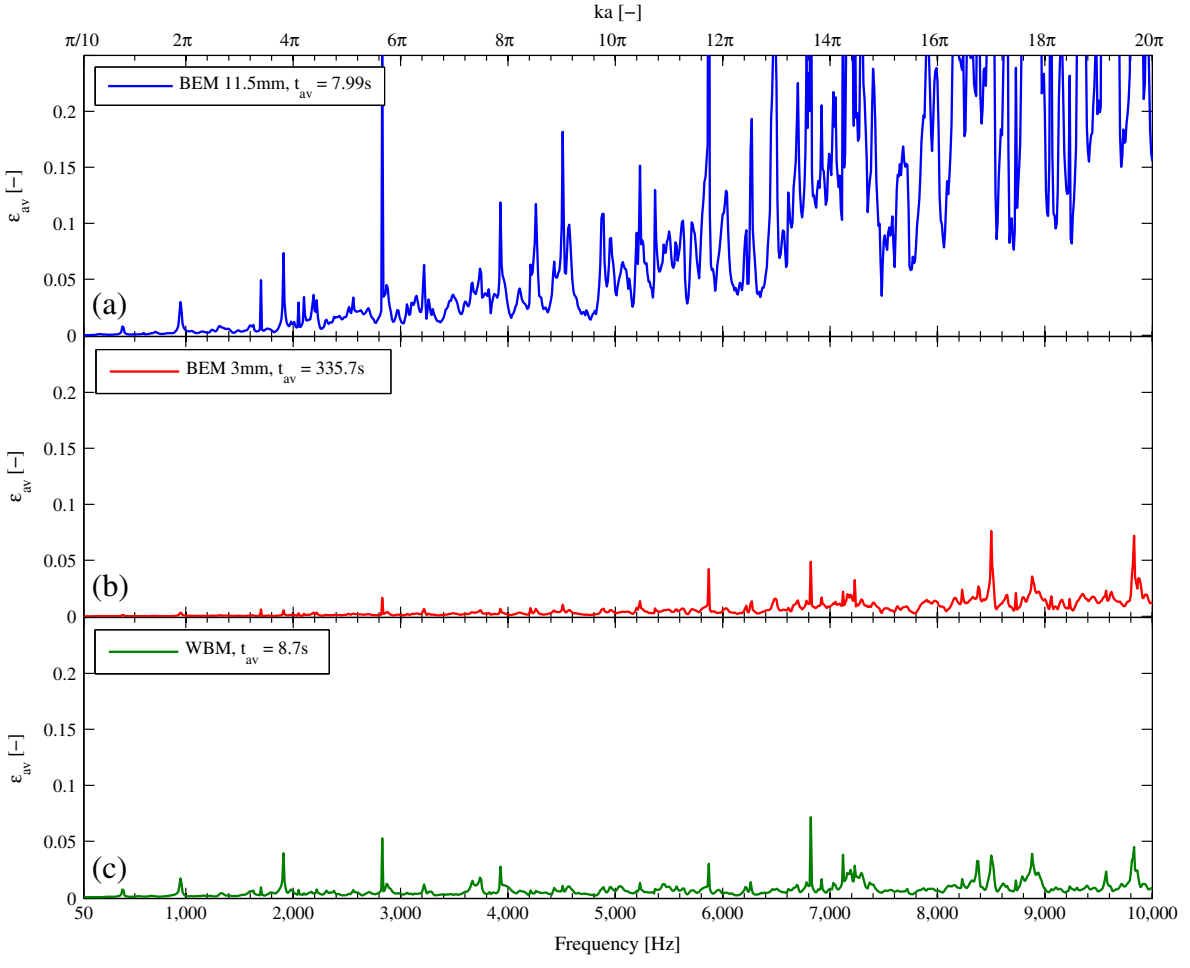

Fig. 14. Validation example 3: average complex acoustic pressure amplitude prediction errors: (a) BEM 11.5 mm, (b) BEM 3 mm, (c) WBM.

obtain the same overall average prediction accuracy as the WBM calculation. This results in an average computation time of 335.7 s per frequency, while the WBM model only needs 8.7 s per frequency to obtain a similar overall prediction accuracy. It can be concluded that for this validation example the newly developed multi-level WBM modelling concept outperforms the BEM by a factor of about 40. This clearly illustrates the computational efficiency potential of the proposed modelling concept.

6. Conclusions

This paper discusses a new multi-level modelling framework for the numerical solution of general two-dimensional acoustic multiple-scattering problems in the low- and mid-frequency range. The proposed approach is based on an existing deterministic Trefftz-based numerical modelling technique, called the Wave Based Method, and is aimed to alleviate or remove some of the geometrical constraints faced when applying this method for the study of unbounded problems with multiple scatterers. The main idea of the approach is to consider the multiple objects in a problem as different 'levels' of the problem. Each level considers the reflection and scattering on the boundaries of one particular object, using existing WBM techniques for unbounded problems. A special compound wave function set and application of the superposition principle for multiple outgoing wave fields through an adapted weighted residual formulation link the different levels, yielding a single multi-level numerical model which governs the entire multiple-scattering problem.

The new method is validated by means of three numerical examples, illustrating both the excellent accuracy and the superior numerical performance as compared to classical element-based numerical modelling techniques. This reduction in computational load, combined with the lack of pollution errors, makes the multi-level WBM particulary suited for the treatment of multiple-scatterer problems in an extended frequency range.

The underlying theoretical basis of the multi-level approach presented in this paper does not rely on particular details of the problem type being solved. As a result, the same approach can be readily extended to other fields of applications (solid dynamics, electro-magnetics, ...) and three-dimensional problems. These extensions are currently being investigated and will be reported on in the near future. Moreover, the extension of this approach to the study of interior problems containing multiple complex shaped inclusions is a topic of current research. Initial results of this investigation have been published in [43].

Acknowledgement

Bert Van Genechten is a doctoral fellow of the Research Foundation Flanders (FWO), Belgium and the research of Bart Bergen is funded by a Ph.D. grant of the Institute for the Promotion of Innovation through Science and Technology in Flanders (IWT-Vlaanderen).

References

[1] P.A. Martin, Multiple Scattering, Interaction of Time-Harmonic Waves with *N* obstacles, Encyclopedia of Mathematics and its Applications, vol. 107, Cambridge University Press, 2006.
[2] P.A. Martin, Integral-equation methods for multiple-scattering problems, I. Acoustics, Quarterly Journal of Mechanics and Applied Mathematics 38 (1) (1985) 105–118, doi:10.1093/qjmam/38.1.105.
[3] P.A. Martin, F.J. Rizzo, Partitioning boundary, integral equations, and exact Green's functions, International Journal for Numerical Methods in Engineering 38 (1995) 3483–3495, doi:10.1002/nme.1620382007.
[4] L.L. Foldy, The multiple scattering of waves. I. General theory of isotropic scattering by randomly distributed scatterers, Physical Review 67 (1945) 107–119, doi:10.1103/PhysRev.67.107.
[5] M. Lax, Multiple scattering of waves, Reviews of Modern Physics 23 (4) (1951) 287–310, doi:10.1103/RevModPhys.23.287.
[6] V. Twersky, Multiple scattering of radiation by an arbitrary configuration of parallel cylinders, The Journal of the Acoustical Society of America 24 (1) (1952) 42–46, doi:10.1121/1.1906845.
[7] P.C. Waterman, New formulation of acoustic scattering, The Journal of the Acoustical Society of America 45 (6) (1969) 1417–1429, doi:10.1121/1.1911619.
[8] B. Peterson, S. Ström, Matrix formulation of acoustic scattering from an arbitrary number of scatterers, Acoustical Society of America 56 (3) (1974) 771–780, doi:10.1121/1.1903325.
[9] P.A. Martin, On connections between boundary integral equations and *T*-matrix methods, Engineering Analysis with Boundary Elements 27 (7) (2003) 771–777, doi:10.1016/S0955-7997(03)00028-6.
[10] W.C. Chew, C.C. Lu, Y.M. Wang, Efficient computation of three-dimensional scattering of vector electromagnetic waves, Journal of the Optical Society of America A 11 (1994) 1528–1537, doi:10.1364/JOSAA.11.001528.
[11] X. Antoine, C. Chniti, K. Ramdani, On the numerical approximation of high-frequency acoustic multiple scattering problems by circular cylinders, Journal of Computational Physics 227 (3) (2008) 1754–1771, doi:10.1016/j.jcp.2007.09.030.
[12] O. Von Estorff, Boundary Elements in Acoustics: Advances and Applications, WIT Press, 2000.
[13] O. Zienkiewicz, R. Taylor, The Finite Element Method – The Three Volume Set, sixth ed., Butterworth-Heinemann, 2005.
[14] I. Harari, E. Turkel, Accurate finite difference methods for time-harmonic wave propagation, Journal of Computational Physics 119 (2) (1995) 252–270, doi:10.1006/jcph.1995.1134.
[15] L.L. Thompson, A review of finite-element methods for time-harmonic acoustics, The Journal of the Acoustical Society of America 119 (3) (2006) 1315–1330, doi:10.1121/1.2164987.
[16] J.B. Keller, D. Givoli, Exact non-reflecting boundary conditions, Journal of Computational Physics 82 (1) (1989) 172–192, doi:10.1016/0021-9991(89)90041-7.
[17] M.J. Grote, J.B. Keller, On nonreflecting boundary conditions, Journal of Computational Physics 122 (2) (1995) 231–243, doi:10.1006/jcph.1995.1210.
[18] P. Bettess, Infinite Elements, Penshaw Press, 1992.
[19] D.S. Burnett, R.L. Holford, An ellipsoidal acoustic infinite element, Computer Methods in Applied Mechanics and Engineering 164 (1–2) (1998) 49–76, doi:10.1016/S0045-7825(98)00046-2.

[20] R.J. Astley, G.J. Macaulay, J.P. Coyette, Mapped wave envelope elements for acoustical radiation and scattering, Journal of Sound and Vibration 170 (1) (1994) 97–118, doi:10.1006/jsvi.1994.1048.
[21] J.-P. Berenger, A perfectly matched layer for the absorption of electromagnetic waves, Journal of Computational Physics 114 (2) (1994) 185–200, doi:10.1006/jcph.1994.1159.
[22] I. Harari, M. Slavutin, E. Turkel, Analytical and numerical studies of a finite element PML for the Helmholtz equation, Journal of Computational Acoustics 8 (1) (2000) 121–137, doi:10.1142/S0218396X0000008X.
[23] M.J. Grote, C. Kirsch, Dirichlet-to-Neumann boundary conditions for multiple scattering problems, Journal of Computational Physics 201 (2) (2004) 630–650, doi:10.1016/j.jcp.2004.06.012.
[24] M.J. Grote, C. Kirsch, Nonreflecting boundary condition for time-dependent multiple scattering, Journal of Computational Physics 221 (1) (2007) 41–62, doi:10.1016/j.jcp.2006.06.007.
[25] P. Bouillard, F. Ihlenburg, Error estimation and adaptivity for the finite element method in acoustics: 2d and 3d applications, Computer Methods in Applied Mechanics and Engineering 176 (1–4) (1999) 147–163, doi:10.1016/S0045-7825(98)00334-X.
[26] R. Freymann, Advanced Numerical and Experimental Methods in the Field of Vehicle Structural-Acoustics, Hieronymus Buchreproduktions GmbH, München, 2000.
[27] S. Marburg, Six boundary elements per wavelength: is that enough?, Journal of Computational Acoustics 10 (1) (2002) 25–51, doi:101142/S0218396X02001401.
[28] W. Desmet, A Wave Based Prediction Technique for Coupled Vibro-Acoustic Analysis, K.U.Leuven, Division PMA, Ph.D. Thesis, 98D12.
[29] E. Trefftz, Ein gegenstück zum ritzschen verfahren, in: Second International Congress on Applied Mechanics, Zürich, Switserland, 1926, pp. 131–137.
[30] C. Vanmaele, D. Vandepitte, W. Desmet, An efficient wave based prediction technique for dynamic plate bending problems with corner stress singularities, Computer Methods in Applied Mechanics and Engineering 198 (30–32) (2009) 2227–2245, doi:10.1016/j.cma.2009.01.015.
[31] C. Vanmaele, D. Vandepitte, W. Desmet, An efficient wave based prediction technique for plate bending vibrations, Computer Methods in Applied Mechanics and Engineering 196 (33–34) (2007) 3178–3189, doi:10.1016/j.cma.2007.03.002.
[32] B. Pluymers, B. Van Hal, D. Vandepitte, W. Desmet, Trefftz-based methods for time-harmonic acoustics, Archives of Computational Methods in Engineering (ARCME) (2007) 343–381, doi:10.1007/s11831-007-9010-x.
[33] W. Desmet, B. Van Hal, P. Sas, D. Vandepitte, A computationally efficient prediction technique for the steady-state dynamic analysis of coupled vibro-acoustic systems, Advances in Engineering Software 33 (7–10) (2002) 527–540, doi:10.1016/S0965-9978(02)00062-5.
[34] B. Pluymers, W. Desmet, D. Vandepitte, P. Sas, On the use of a wave based prediction technique for steady-state structural-acoustic radiation analysis, Computer Modeling in Engineering and Sciences 7 (2) (2005) 173–184.
[35] D. Colton, R. Kress, Inverse Acoustic and Electromagnetic Scattering Theory, second ed., Springer-Verlag, Berlin, Heidelberg, New York, 1998.
[36] B. Pluymers, Wave Based Modelling Methods for Steady-State Vibro-Acoustics, K.U.Leuven, Division PMA, Ph.D. Thesis, 2006D04.
[37] J.-D. Benamou, B. Després, A domain decomposition method for the helmholtz equation and related optimal control problems, Journal of Computational Physics 136 (1) (1997) 68–82, doi:10.1006/jcph.1997.5742.
[38] I. Herrera, Boundary Methods: An Algebraic Theory, Pitman Adv. Publ. Program, London, 1984.
[39] B. Bergen, B. Van Genechten, B. Pluymers, D. Vandepitte, W. Desmet, Efficient wave based models for acoustic scattering and transmission problems using point source and plane wave excitation, in: Proceedings of the Fourteenth International Congress on Sound and Vibration (ICSV14), Cairns, Australia, 2007.
[40] T. Huttunen, P. Gamallo, R.J. Astley, Comparison of two wave element methods for the Helmholtz problem, Communications in Numerical Methods in Engineering 25 (2009) 35–52, doi:10.1002/cnm.1102.
[41] A.P. Zielinski, I. Herrera, Trefftz method: fitting boundary conditions, International Journal for Numerical Methods in Engineering 24 (1987) 871–891, doi:10.1002/nme.1620240504.
[42] F. Ihlenburg, Finite Element Analysis of Acoustic Scattering, Applied Mathematical Sciences, vol. 132, Springer-Verlag, New York, 1998.
[43] B. Van Genechten, K. Vergote, D. Vandepitte, W. Desmet, A multi-level wave based numerical modelling framework for the steady-state dynamic analysis of bounded Helmholtz problems with multiple inclusions, Computer Methods in Applied Mechanics and Engineering 199 (29–32) (2010) 1881–1905, doi:10.1016/j.cma.2010.01.013.